Protein Fluctuations, Distributed Coupling, and the Binding of Ligands to Heme Proteins

V. Šrajer, L. Reinisch, and P. M. Champion*

Contribution from the Department of Physics, Northeastern University, Boston, Massachusetts 02115. *Received October 30, 1987*

Abstract: A general model for the binding of small molecules to heme proteins is presented. The model is based on a potential surface involving the iron-ligand binding coordinate, r, and an internal protein coordinate, Q (e.g., iron-porphyrin out-of-plane displacement). A protein fluctuation coordinate, x, is used to modulate the coupling (iron out-of-plane equilibrium position) of the unligated state of the system. A Gaussian distribution in the out-of-plane equilibrium position has been previously shown to account for the non-Gaussian inhomogeneous broadening of the deoxy myoglobin Soret band (Šrajer et al. *Phys. Rev. Lett.* **1986**, *57*, 1267). We propose that this distribution is driven by protein conformational fluctuations that are frozen into the ensemble at low temperature (quenched disorder) leading directly to the inhomogeneous distribution in the geminate rebinding kinetics observed by Austin et al. (*Biochemistry* **1975**, *14*, 5355). Specific example calculations involving the low-temperature geminate recombination of CO to myoglobin and leghemoglobin are discussed in detail and a simple intuitive picture is presented that separates the activation enthalpy into distal pocket, H_D, and proximal, H_P, terms. The proximal term involves the work needed to bring the iron atom to the in-plane transition state. At physiological temperatures, when the fluctuations are rapid with respect to the kinetic time scales, the observed single exponential rate and the corresponding Arrhenius barrier height are predicted from the low-temperature kinetic parameters. These parameters, along with other experimental and theoretical constraints, are used to construct detailed potential energy surfaces that are useful in further investigations of ligand binding to heme proteins. As an example, we present an analysis of hemoglobin cooperativity in the Appendix. It is suggested that the protein conformations associated with the R and T states will couple differently to the unligated iron-porphyrin coordinate. Such differences in coupling can be envisioned as larger and more discrete versions of the fluctuations that drive the distributions in coupling found for the monomeric myoglobin system. It is shown that significant amounts of energy can easily be stored in the Stokes shift difference associated with the unligated T and R hemes. Such nuclear relaxation effects may have already been detected experimentally in magnetic susceptibility and kinetics experiments. The observed values for the relative "on" and "off" rates of the R and T states are in accord with the proposed potential surfaces.

I. Introduction

The protein structure-function relationships involved in the binding of ligands to heme proteins have been the focus of a wide variety of physical, biological, and chemical investigations during the last several decades. A well-studied process from an experimental point of view is the geminate recombination of CO to myoglobin (Mb) at low ($T \leq 160$ K) temperature.[1,2] Quantum effects, such as tunneling, are observed below ~60 K.[3,4] Above ~160 K, the CO ligand can begin to diffuse through the protein matrix and eventually into the solvent,[5] leading to more complicated effects. For the moment, we focus on the relatively simple geminate process:

$$\text{Mb·CO} \underset{\{k\}}{\overset{\gamma}{\rightleftharpoons}} \text{Mb} + \text{CO} \qquad (1)$$

Equation 1 denotes the photolysis of carbon monoxy myoglobin (Mb·CO) by light (γ) and the subsequent rebinding ($\{k\}$). The curly brackets around the $\{k\}$ indicate that a single rate is not sufficient to describe the rebinding and that a distribution in rates is necessary to explain the nonexponential kinetics observed at low temperature. The distribution of rates is thought[6] to arise from conformational substates of the myoglobin that are frozen into the ensemble below the phase transition of the solvent (quenched disorder). At physiological temperatures, when rapid fluctuations of the protein become possible, the system can be described by averaging over the fluctuation coordinates and the observed simple exponential relaxation should be predicted from the low-temperature distribution.

Several theoretical approaches have been previously applied to this problem,[7-11] and we will attempt to incorporate and discuss the various points of view as they pertain to the present treatment. We remark at the outset that the formal aspects of the model given here draw deeply from the previous work.[7-9] Nevertheless, fundamental differences arise due to the different dimensionalities of the treatments. Buhks and Jortner[9] calculate the low-temperature rates within a single-dimensional harmonic space and do not attempt to introduce the (protein) fluctuations. Agmon and Hopfield[7] and Bowne and Young[8] utilize a two-dimensional space composed of the iron-CO binding coordinate (r) and a generalized protein coordinate (X). In these models the generalized protein is treated with a *single* coordinate and it is not possible to consider the relaxation and energetics of the important iron-porphyrin coordinate separately from the rest of the protein. In the present model, we employ a three-dimensional approach that explicitly exposes the iron-porphyrin coordinate (Q) along with the rest of the generalized protein (x). We allow for coupling between these protein coordinates so that fluctuations in x can affect the equilibrium position of Q. We suggest that the ca. 0.45 Å distance that the iron must move (relative to the porphyrin) during the binding process contributes important terms to the free energy of the transition state. Moreover, we allow this coordinate to relax to an out-of-plane geometry, even at low temperature, when the rest of the protein is frozen (x held constant). This approach predicts the observed high-temperature single-exponential rebinding rate directly from the low-temperature distribution. In contrast, the Agmon-Hopfield (AH) model fails in the high-temperature prediction. This arises from the fact that

(1) Austin, R. H.; Beeson, K.; Eisenstein, L.; Frauenfelder, H.; Gunsalus, I. C.; Marshall, V. P. *Phys. Rev. Lett.* **1974**, *32*, 403-407.
(2) Austin, R. H.; Beeson, K. W.; Eisenstein, L.; Frauenfelder, H.; Gunsalus, I. C. *Biochemistry* **1975**, *14*, 5355-5373.
(3) Alberding, N.; Austin, R. H.; Beeson, K. W.; Chan, S. S.; Eisenstein, L.; Frauenfelder, H.; Nordlund, T. M. *Science* **1976**, *192*, 1002-1004.
(4) Alben, J. O.; Beece, D.; Bowne, S. F.; Eisenstein, L.; Frauenfelder, H.; Good, D.; Marden, M. C.; Moh, P. P.; Reinisch, L.; Reynolds, A. H.; Yue, K. T. *Phys. Rev. Lett.* **1980**, *44*, 1157-1160.
(5) Ansari, A.; Dilorio, E. E.; Dlott, D. D.; Frauenfelder, H.; Iben, I. E. T.; Langer, P.; Roder, H.; Sauke, T.; Shyamsunder, E. *Biochemistry* **1986**, *25*, 3139-3146.
(6) Ansari, A.; Berendzen, J.; Bowne, S. F.; Frauenfelder, H.; Iben, I. E. T.; Sauke, T. B.; Shyamsunder, E.; Young, R. D. *Proc. Natl. Acad. Sci. U.S.A.* **1985**, *82*, 5000-5004.
(7) Agmon, N.; Hopfield, J. J. *J. Chem. Phys.* **1983**, *79*, 2042-2053.
(8) Young, R. D.; Bowne, S. F. *J. Chem. Phys.* **1984**, *81*, 3730-3737.
(9) Buhks, E.; Jortner, J. *J. Chem. Phys.* **1985**, *83*, 4456-4462.
(10) Stein, D. L. *Proc. Natl. Acad. Sci. U.S.A.* **1985**, *82*, 3670-3672.
(11) Bialek, W.; Goldstein, R. F. *Biophys. J.* **1985**, *48*, 1027-1044.

0002-7863/88/1510-6656$01.50/0

the X coordinate is held constant on the rebinding trajectory at low temperature. Thus, even in a "sudden" approximation, when the iron is assumed to relax instantaneously to a new equilibrium position, there are no terms in the AH potential to account for the energy of this relaxation. Finally, we note that the energetically significant relaxation in Q leads directly to a quadratic rather than a linear mapping of the Gaussian fluctuations into a barrier height distribution function. The resulting barrier height distribution functions are naturally skewed and in accord with experimental observation,[1-6] rather than Gaussian as predicted by the AH model. The importance of quadratic energy mapping and non-Gaussian distribution functions in high-spin ferrous heme proteins has been explored previously and found to be necessary in order to account for the optical properties of the Soret Band.[12]

Surprisingly, the expansion of the theoretical base to include a third coordinate does not further complicate the picture. Rather, it leads directly to very simple, intuitive, and easily visualized results. Moreover, many of the parameters in the present theory can be related to other types of experiments (e.g., X-ray, Mössbauer, EXAFS, electronic absorption, Raman, and infrared spectroscopies) and incorporated into a general framework that describes the rebinding kinetics. In contrast, the previous theories[7,8] rely heavily on the conceptual coordinates (e.g., X) and cannot be constrained by additional independent experiments.

We wish to stress that the main purpose of this work is not to simply fit the low-temperature rebinding kinetics, but rather to develop a method of data analysis that allows the information derived from kinetic experiments to be related to fundamental aspects of the actual ligand binding potential. The potential surface can then be constructed by incorporation of the kinetic results along with other experimental and theoretical constraints. In Appendix A we demonstrate that such potential surfaces can be utilized to examine how protein structure can control ligand binding through its coupling to the iron–porphyrin coordinate in hemoglobin. For example, we show how small differences in the force constants and equilibrium positions for the R and T states of hemoglobin (Hb) can result in significant cooperative free energy localized at the *unligated* heme. Thus, we suggest that the model presented here is useful in making direct structure–function correlations in heme proteins.

In the following section we will briefly discuss some general concepts involving distributed relaxation and present a simple intuitive picture. The formal treatment follows, with explicit expressions derived for the rebinding parameters in terms of detailed potential energy surfaces. Section III presents the results of fitting the low-temperature rebinding kinetics. In section IV we compare the fitting parameters with other data and suggest some possible experiments that might help to determine more quantitatively the relevant potential energy surfaces. Finally, we discuss in detail the differences and similarities between this and other models.

II. Theory

A. Distributed Relaxation. The general concept of distributed relaxation pervades most subfields of physics and chemistry that involve glassy or amorphous systems.[13] We have recently been drawn into this area through resonant light-scattering studies of heme proteins.[14] In particular, we have suggested that distributions in the nonradiative decay of the π–π^* excitations of the heme chromophore in cytochrome c may lead to anomalous resonance enhancement of the Rayleigh scattering.[14,15] In general, one can write the relaxation function for an ensemble of simply relaxing systems as

$$\phi(t) = \int P(\Gamma)e^{-\Gamma t}\,d\Gamma \qquad (2)$$

where Γ represents the exponential decay constant (i.e., damping factor or rate constant) of a correlation and $P(\Gamma)\,d\Gamma$ is the probability of finding a molecule with a particular Γ. In the case of nonradiative decay of an electronic excitation of the heme, the time scale for decay can be extremely fast (10^{-13}–10^{-14} s). Quite often it is *assumed* that $P(\Gamma) = \delta(\Gamma - \Gamma_0)$ and single-exponential decay dominates the ensemble.

The same basic approach holds for the rebinding of CO to Mb in eq 1. If we identify $N(t)$ with the normalized concentration of Mb (unbound) following the flash photolysis (γ), we can write by analogy

$$N(t) = \int P(k)e^{-kt}\,dk \qquad (3)$$

A similar formalism used by Frauenfelder et al.[1-6] will be employed here:

$$N(t) = \int g(H)e^{-k(H)t}\,dH \qquad (4)$$

with

$$k(H) = k_0e^{-H/k_BT} \qquad (5)$$

At temperatures above the tunneling regime ($T \geq 60$ K), the rate constant $k(H)$ is assumed to vary in the usual classical (Arrhenius) way with barrier height (H). The quantity $g(H)\,dH$ describes the probability of finding a Mb molecule in the frozen matrix with a barrier height between H and $H + dH$. Frauenfelder et al.[1-6] have shown that $g(H)$ is *not* a delta function, and by using eq 4 and inverse Laplace transform techniques they have determined the $g(H)$'s for a wide variety of heme protein systems.

B. Intuitive Approach. The intuitive model rests upon our ability to identify the configurational coordinate that plays a dominant role in determining the rebinding barrier height. This special coordinate is one of many protein coordinates that fluctuate above the freezing point (T_f) and are found in a static distribution below T_f. We parametrize the problem with respect to this coordinate and its distribution in coordinate space. This approach has worked well in other contexts,[12-15] and we proceed following the same logic. In part C of this section we will formally relate these expressions to explicit potential energy surfaces of the heme–ligand system.

We first consider the work needed to bring the Mb into a "transition" state for binding the CO. By analogy to various other chemical systems (e.g., the inversion of ammonia), it seems probable that a key coordinate involves the iron displacement toward the porphyrin center (distance ca. 0.45 Å). We assume that the work involved in bringing the iron porphyrin system into the planar transition-state configuration can be written as

$$H_P = \tfrac{1}{2}Ka^2 \qquad (6)$$

where the "force constant" K is yet to be determined, but involves all linear restoring forces between the iron–protein and iron–porphyrin. The parameter a denotes the overall displacement of the relative iron–porphyrin coordinate (Q) that is needed to bring the system from the unligated configuration to the in-plane geometry. We shall refer to this term as the "proximal" work.

In addition to eq 6, there is another term that contributes to the total barrier height. We refer to this term as the "distal pocket" work. It may involve a variety of effects (e.g., the work needed to tilt the CO molecule off the preferred linear binding geometry, Fe–CO bond stabilization forces involving non-covalent interactions between CO and the distal pocket, work involved in "unsticking" the CO from the pocket, etc.). All distal pocket forces involved in the approach of the CO to the transition state need to be included in this second term. We denote this term as H_D and write for the total barrier height

$$H(a) = \tfrac{1}{2}Ka^2 + H_D \qquad (7)$$

The distribution in the barrier heights arises from a distribution of protein conformations, frozen into the ensemble below T_f, leading to a distribution of iron–porphyrin geometries in the photolyzed deoxy state. This results in different displacements

(12) Šrajer, V.; Schomacker, K. T.; Champion, P. M. *Phys. Rev. Lett.* **1986**, *57*, 1267–1270.
(13) Klafter, J.; Shlesinger, M. F. *Proc. Natl. Acad. Sci. U.S.A.* **1986**, *83*, 848–851.
(14) Schomacker, K. T.; Šrajer, V.; Champion, P. M. *J. Chem. Phys.* **1987**, *86*, 1796–1802.
(15) Reinisch, L.; Schomacker, K. T.; Champion, P. M. *J. Chem. Phys.* **1987**, *87*, 150–158.

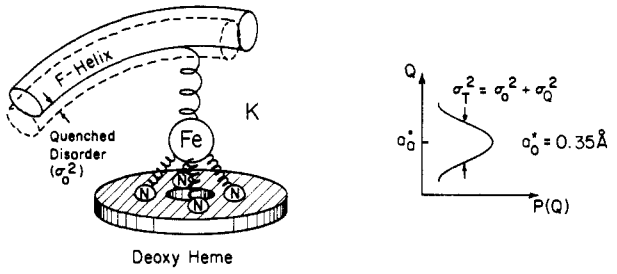

Figure 1. A schematic diagram showing the source of the "proximal pocket work" H_P. The constant K represents all linear restoring forces involved in displacing the iron porphyrin system toward the planar transition state. The total iron–porphyrin disorder, σ_T^2, is presented as a sum of two contributions: fast local motion of the iron atom, σ_Q^2, and a "static" frozen ensemble contribution, σ_a^2. For the photolized Mb, we take $a_0^* = 0.35$ Å.

(a) to bring the iron atom to the in-plane geometry. The fact that the iron displacements are significantly distributed in deoxy Mb is indicated by a variety of X-ray and Mössbauer studies[16,17] as well as by the optical absorption spectra.[12] Fast local motion ($\tau \leq 10^{-12}$ s, denoted by σ_Q in Fig. 1) of the iron atom is not included in the distribution since it can be averaged out of the relatively slow rebinding kinetics ($\tau > 10^{-9}$ s). However, such (fast) motion may need to be included in the inhomogeneous broadening of the electronic absorption band[12] since the nonradiative electronic relaxation processes have time scales comparable to the nuclear motion. In any case, the "static" contribution to the iron–porphyrin disorder is expected to dominate the high-frequency local motion. We take the distribution of the iron displacement to be Gaussian

$$P(a) = \frac{1}{\sigma_a\sqrt{2\pi}} e^{-(a-a_0^*)^2/2\sigma_a^2} \tag{8}$$

with a_0^* denoting the average out-of-plane iron–porphyrin displacement in the photolyzed deoxy state. A schematic diagram of the situation is shown in Figure 1. The distribution of barrier heights, $g(H)$, is found directly from eq 8 along with the parametric eq 7 by using

$$g(H) = P(a)\left|\frac{da}{dH}\right| \tag{9}$$

This leads to

$$g(H) = \frac{(H - H_D)^{-1/2}}{2\sigma_a\sqrt{\pi K}} \times \left[\exp\left(-\frac{(\sqrt{H - H_D} - a_0^*\sqrt{K/2})^2}{K\sigma_a^2}\right) + \exp\left(-\frac{(\sqrt{H - H_D} + a_0^*\sqrt{K/2})^2}{K\sigma_a^2}\right)\right] \tag{10}$$

which is essentially the same distribution that was used in fitting the Soret band line shape of deoxy Mb.[12]

We note that the second term in eq 10 arises from the fact that, within the harmonic and Gaussian approximations of the model, there is a finite probability of finding energy barriers with $H > H_D$ when the iron atom is displaced to the distal side of the heme ($a < 0$). A more general model could acknowledge the possibility of non-Gaussian distributions in the iron displacement as well as anharmonic restoring forces; however, such generalizations will not be considered here. For the experimental cases examined in this study, the effect of the second term in eq 10 is negligible.

The calculation of the observable quantity, $N(t)$, is straightforward. We write

$$N(t) = \int_{H_D}^{\infty} g(H)\exp(-k_0 t e^{-H/k_BT})\,dH \tag{11}$$

where we note that $g(H) = 0$ if $H < H_D$ and we have combined eq 4 and 5. We also see that

$$\exp(-k_0 t e^{-H/k_BT}) = \exp(-e^{(H' - H)/k_BT}) \equiv \Theta(H - H') \tag{12}$$

where

$$H' = k_BT \ln(k_0 t) \tag{13}$$

The function $\Theta(H - H')$ closely approximates a step function at H' so that to a good approximation

$$N(t) \cong \int_{H'}^{\infty} g(H)\,dH \tag{14}$$

If $H' < H_D$ we have $N(t) = 1$ via normalization. If $H' > H_D$ we find a closed form expression for $N(t)$

$$N(t) \cong \frac{1}{2}\left[\operatorname{erfc}\frac{\sqrt{H' - H_D} - a_0^*\sqrt{K/2}}{\sigma_a\sqrt{K}} + \operatorname{erfc}\frac{\sqrt{H' - H_D} + a_0^*\sqrt{K/2}}{\sigma_a\sqrt{K}}\right] \tag{15}$$

where erfc is the complementary error function (1 − erf) and H' is given by eq 13. Equation 15 provides a convenient approximation to the observed $N(t)$ and allows for efficient fitting of data via least-squares analysis. The approximation can be checked by direct numerical integration of eq 11.

C. Formal Development. In this section, we assume that the general eq 4 and 5 hold, and that the effects of friction and entropy can be transferred to k_0, the ubiquitous prefactor.[18] The effects of quantum mechanical processes can, in principle, be included in the calculation by the introduction of a transmission function, T (which allows penetration of the barrier), before the integration in phase space. In the event that T is a step function, eq 5 will result and is a generally accepted starting point. We will not attempt the tunneling calculations here, since the potential surfaces are not yet known in enough detail to provide unambiguous results (see ref 9 for a one-dimensional nonadiabatic calculation of tunneling rates). Our main goal is to show that the intuitive eq 7 and the average over $P(a)$ (eq 8) are, in fact, rather general results based on explicit potential surfaces and the coupling of protein fluctuations to the heme. We also derive expressions relating the parameters in eq 7 and 8 to the explicit potential energy surfaces.

We assume that binding of CO to Mb involves only two spin states. Thus, the $S = 2$ spin quintet (q) electronic state of the iron in Mb is converted directly into the $S = 0$ spin singlet (s) of Mb·CO without the intervention of the $S = 1$ spin triplet (t) state. This assumption may prove to be incorrect in some circumstances, since it is quite likely that the triplet state is nearby and is probably involved in the O_2 binding reaction.[19] Nevertheless, we outline the simplest possible model and hold to a two-surface problem. An additional triplet surface could, in principle, be added to the model with the possibility of intersections leading to a q → t → s rebinding sequence.

We use a notation similar to, and draw heavily on, the insightful analysis of Agmon and Hopfield.[7] Nevertheless, we believe it is necessary to explicitly expose the relative iron–porphyrin coordinate, Q, which is not considered in their analysis. This coordinate is free to vary as evidenced by the fact that the iron atom moves into the plane upon CO binding and out of the plane upon photolysis, *even at low temperature*. The AH model does not include

(16) Frauenfelder, H.; Petsko, G. A.; Tsernoglou, D. *Nature (London)* **1979**, *280*, 558–563.
(17) Parak, F.; Knapp, E. W. *Proc. Natl. Acad. Sci. U.S.A.* **1984**, *81*, 7088–7092.
(18) Frauenfelder, H.; Wolynes, P. G. *Science* **1985**, *229*, 337–345.
(19) Olafson, B.; Goddard, W. In *Hemoglobin and Oxygen Binding*; Chien Ho, Ed.; Elsevier: New York, 1982; pp 83–89.

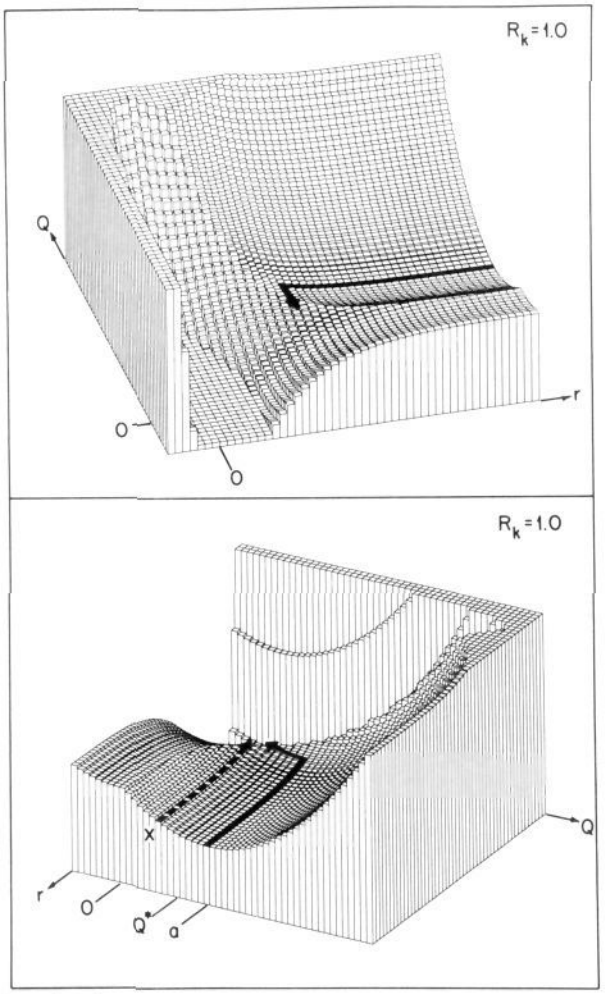

Figure 2. The minimum energy surface as a function of r and Q for $R_k = 1$. The surface is viewed from two different angles and is truncated at the bottom (at −55 kJ mol^{-1}) and at the top (at 65 kJ mol^{-1}) for better display of the energy barrier. The energy surface shown is for r between −0.4 and 2.5 Å and for Q between −0.2 and 1.0 Å. The parameters used are the following: $k_q = k_s = 65$ N m^{-1}, $R_D = 1.16$, $D_s = 111.2$ kJ mol^{-1}, $\Delta = 23.2$ kJ mol^{-1}, $\beta = 2.8$ Å^{-1}, $a = 0.35$ Å. The solid arrow denotes a convenient path of integration for evaluating the energy barrier at the transition state. The dashed arrow corresponds to the recombination path according to the AH model[7] where X replaces Q and is held fixed on the rebinding trajectory.

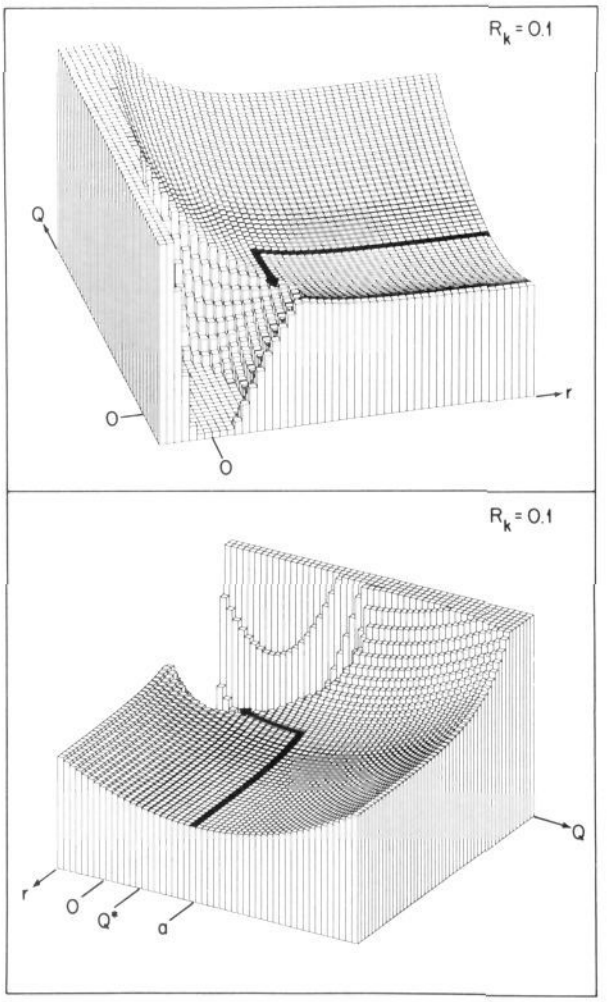

Figure 3. The minimum energy surface as a function of r and Q for $R_k = 0.1$. The surface in truncated at the bottom at −90 kJ mol^{-1} and at the top at 30 kJ mol^{-1}. The parameters are the following: $k_q = 26$ N m^{-1}, $R_D = 2.9$, $D_s = 135.6$ kJ mol^{-1}, $\Delta = 47.6$ kJ mol^{-1}, $\beta = 2.5$ Å^{-1}, $a = 0.35$ Å. Everything else is the same as for Figure 2.

this motion explicitly and this eliminates the possibility of treating the iron, porphyrin, and ligand as a three-body system, modulated by the protein fluctuations.

We write for the potential of the singlet surface

$$V_s(r,Q,x) = D_s[e^{-2\beta r} - 2e^{-\beta r}] + \tfrac{1}{2}k_sQ^2 + \tfrac{1}{2}f_s(x - x_0)^2 \qquad (16)$$

where r is the deviation of the Fe–CO bond length from equilibrium, D_s is the depth of the Morse potential well, and β is the curvature. D_s and β can be adjusted to give a harmonic force constant near the bottom of the well that supports the observed ~500 cm^{-1} Fe–CO vibrational frequency. The quantity k_s is a force constant describing a harmonic approximation to the potential which maintains the iron atom in the plane of the porphyrin. The last term explicitly acknowledges that the total system energy also depends upon global contributions of the protein coordinate, x, through a weak force constant, f_s, describing a harmonic approximation to the many atomic degrees of freedom of the protein.

The quintet potential surface is given by

$$V_q(r,Q,x) = D_qe^{-\beta r} - \Delta + \tfrac{1}{2}k_q(Q - a)^2 + \tfrac{1}{2}f_qx^2 \qquad (17)$$

where $D_qe^{-\beta r}$ represents the repulsion energy of the quintet state as the CO molecule approaches. The quantity Δ gives the energy separation between the minima of the harmonic surfaces of the two spin states at infinite iron–CO separation (the q state is stabilized by Δ). The third term represents the harmonic potential of the deoxy iron atom with respect to the porphyrin plane. The equilibrium position, a, is ca. 0.45 Å and the fact that $R_k \equiv k_q/k_s$ may differ from unity allows for the possibility of quadratic as well as linear coupling between the two spin states. Figures 2 and 3 show the minimum energy surfaces as a function of Q and r for $R_k = 1$ and 0.1. Figure 8 in the Appendix shows some 2-dimensional sections of the potential surfaces and may help in visualizing the effects of the various parameters.

The protein fluctuations are treated in the following way. To a first approximation we have allowed the global conformational energy to be described by a quadratic function of protein "coordinate", x

$$E_{cq} = \tfrac{1}{2}f_qx^2 \text{ (quintet)} \qquad (18a)$$

$$E_{cs} = \tfrac{1}{2}f_s(x - x_0)^2 \text{ (singlet)} \qquad (18b)$$

where x_0 represents the conformational "shift" in equilibrium position of the globin upon ligand binding. This approach may be justified, in a limited sense, in view of the success of quadratic approximations to the potential of mean force, which implicitly include anharmonic effects.[20] We point out again at this stage

(20) (a) McCammon, J. A.; Wolynes, P. G.; Karplus, M. *Biochemistry* **1979**, *18*, 927–942. (b) McCammon, J. A. *Rep. Prog. Phys.* **1984**, *47*, 1–46. (c) Levy, R. M.; Srinivasan, A.; Olson, W.; McCammon, J. A. *Biopolymers* **1984**, *23*, 1099–1112.

that the coordinate x, as used in this work, is a subspace of the coordinate X as used by Agmon and Hopfield. Taken together x and Q span the full space of X. In addition, we have allowed the force constants f_q and f_s to differ in general. In the case of myoglobin we take $f_q = f_s = f$, since it turns out that the only effect of the conformational terms is to dictate a Gaussian density in x, which is ultimately reflected as a Gaussian distribution of the iron–porphyrin equilibrium position. The quantities f_q and f_s determine the relative widths of these distributions and, if different, can affect the predicted high-temperature rates. Since there are no large tertiary structure changes in Mb, and the protein is free to relax, we consider $f_q = f_s$ to be a reasonable approximation. In the case of hemoglobin, these terms play a much more important role since E_{cs} will carry important strain interactions that develop between the heme and proximal pocket residues in the ligated T state (see Appendix A).

We allow for the direct coupling between the global protein coordinate, x, and the local heme region of the deoxy state by expressing the relative equilibrium position between iron and porphyrin as a linear function of x. (This is analogous to the Duschinsky coupling of the "normal modes" Q and x.) Upon freezing the solution, the protein fluctuation coordinates are "quenched" at random positions and no longer vary within measurable time scales. For a specific photolyzed quintet state molecule, with protein coordinate frozen at x, the expression for the relative equilibrium position between Fe and porphyrin is written as

$$a(x) = a_0^* + \alpha(x - x_0) \tag{19}$$

where we have assumed that the globin is frozen in the ligand bound singlet state with x_0 as the most probable value for the protein coordinate. The quantity a_0^* is the average iron–porphyrin out-of-plane displacement for the Mb photolyzed at low temperature.

The effect of the protein fluctuation coordinate on the iron–porphyrin equilibrium position is expected to be much more important in the unligated state than in the ligated state. In the ligand bound state the width of the iron–porphyrin distribution should be quite small since the iron atom is "locked" into the heme plane by the CO molecule. Thus, in eq 16, we have implicitly allowed the protein–heme coupling parameters to vanish in the singlet state (i.e., $\alpha_{singlet} \equiv 0$). This fixes the iron–porphyrin equilibrium position at $Q = 0$ for all ligated molecules in the ensemble and effectively decouples Q from the protein fluctuations when the ligand is bound. The relative absence of inhomogeneous broadening in the Soret band of Mb·CO[12] strongly supports this simplification and stands in marked contrast to the severe inhomogeneous broadening (due to iron–porphyrin disorder) observed in the unligated species.[12]

In order to be consistent with a homogeneous ensemble of hemes in the ligated state, we consider the Q-dependent terms that govern the localized heme energy in eq 16 and 17. Homogeneity at the ligand bound iron site requires that the energy gap between the singlet and quintet spin states ($V_q(0,0) - V_s(0,0) = D_s + D_q - \Delta + {}^1/_2 k_q a^2$) remains constant for all molecules in the ensemble. Since $a(x)$ carries conformation dependence through x, we set $\Delta = \Delta_v + {}^1/_2 k_q a^2$ in order to ensure homogeneity in the bound state. The fixed quantity, Δ_v, corresponds to the vertical transition energy between spin states at $Q = 0$ and $r = \infty$. The term ${}^1/_2 k_q a^2$, associated with Δ, is referred to as the Stokes shift and represents the nuclear relaxation energy associated with a change of electronic state. Since the Stokes shift is dependent on the protein conformation, this leads to an important source of protein structural control in both the kinetics and energetics of ligand binding (see Appendix A).

The major effect of the protein fluctuations on the ligand binding kinetics arises through the modulation of $a(x)$. The effect appears in the heme localized q-state harmonic surfaces at low temperature because different protein conformations are frozen (or "quenched") into the ensemble. These conformations lead to different iron–porphyrin "equilibrium" displacements after photolysis. The main role of the remaining conformational energy terms, eq 18, is to dictate a Gaussian density in x (and, thus, $a(x)$). The direct energetic contribution of these terms turns out to be small (${}^1/_2 f x_0^2 \ll {}^1/_2 k_q a_0^2$) and, even if explicitly retained, they do not alter the basic mathematical structure of eq 7–10 or the fits to the low-temperature recombination data. As a result, we feel justified in dropping these terms in our treatment of Mb kinetics in order to minimize the numer of unknown parameters.[21] If we take x_0 to be small, but non-zero, and $f \ll k_q$, we can thus neglect the x-dependent terms in eq 16 and 17 and still allow for the possibility of protein diffusion from $\langle x \rangle = x_0$ to $\langle x \rangle = 0$ when $T \geq T_f$[7]. This will cause the mean out-of-plane displacement to be a temperature-dependent quantity (via eq 19). The appealing aspect of this approach is that it allows a_0^* to be smaller than 0.45 Å in the low-temperature photodissociated state and can still account for a well-defined relaxation to the full out-of-plane displacement at room temperature. It should be noted that the case of Hb is much more complicated and the strain energies involved in the ligated T state must be included, via the terms in eq 18 (see Appendix A).

After dropping the x-dependent terms, we equate eq 16 and 17 to find the equation governing the intersection of the two surfaces (footnote 21 discusses the results if the x-dependent terms are included). We employ the same linear approximation as AH[7] which amounts to a choice of parameters that satisfy

$$e^{-\beta r_0} \ll 2 + D_q/D_s \tag{20}$$

where r_0 is the Fe–CO coordinate at the intersection. We also determine the equation for the barrier height, $H(Q,r_0)$, with respect to the Fe–porphyrin coordinate, Q, by using

$$H(Q,r_0) = V_q(Q,r_0) - V_q(a,\infty) \tag{21}$$

This leads to

$$H(Q,r_0) = D_q e^{-\beta r_0} + {}^1/_2 k_q (Q - a)^2 \tag{22}$$

where the last term arises from the allowed relaxation in Q ($Q = a$ at $r \to \infty$) and cannot be recovered from the development of ref 7 (where X is held constant for all r). Equation 22 can now be substituted into the equation for the intersection of the two surfaces, giving

$$H(Q) = (2R_D + 1)^{-1}[\Delta + R_D k_q (Q - a)^2 + {}^1/_2 k_s Q^2] \tag{23}$$

where the r_0 dependence is conveniently eliminated via the approximation (eq 20). The quantity $R_D = D_s/D_q$ relates the relative attraction and repulsion energies for the s and q states as the CO and iron atom approach each other. The transition-state coordinate is found by minimizing eq 23 using $\partial H(Q)/\partial Q|_{Q^*} = 0$. The result is

$$Q^* = \frac{2R_k R_D}{1 + 2R_k R_D} a \tag{24}$$

with $R_k = k_q/k_s$ a measure of the quadratic coupling of the harmonic wells. When Q^* is substituted into eq 23 we find the barrier height is given by eq 7

$$H = H(Q^*) = {}^1/_2 K a^2 + H_D \tag{25}$$

with

$$K = \frac{2R_D R_k + 2R_D + 1}{(2R_D R_k + 1)(2R_D + 1)} k_q \tag{26}$$

and

(21) If we carry the x-dependent terms in eq 16 and 17 through the entire analysis, the general eq 7–11 are unaffected. Equations 19, 26–28, and 33 also apply so long as a_0 and Δ_v are replaced by the new (primed) quantities

$$a_0' = a_0 - f x_0/[K\alpha(2R_D + 1)]$$

$$\Delta_v' = \Delta_v \pm f x_0^2/2 + K(2R_D + 1)(a_0^2 - a_0'^2)/2$$

(where + and − signs correspond to $a_0^\dagger$ and a_0^*, respectively, and $f_q = f_s = f$). The main drawback of this most general approach is that the quantities x_0 and f have only conceptual meaning at this stage and they cannot be independently measured.

$$H_D = \Delta_v/(2R_D + 1) \quad (27)$$

where the vertical transition at $r \rightarrow \infty$ between q and s states (Δ_v) has been held constant in the $Q = 0$ configuration. (The complicated pre-factor in eq 26 is typically of order unity.) If necessary, additional aspects of the distal pocket can be modelled by allowing for steric or electrostatic interactions between the unbound CO molecule and the distal residues. We then write

$$H_D = \Delta_v/(2R_D + 1) + H_S \quad (28)$$

where H_S describes the possibility of a "sticking" interaction between the unbound CO and the pocket. It is worth noting that important details of the bound CO geometry and pocket polarization can be accounted for by variation of the parameters D_s and D_q. The parameter Δ_v is directly related to the crystal field of the pentacoordinate iron atom and can influence H_D through proximal interactions. In this respect, the formal development differs from the intuitive results and shows that a complete separation of the distal and proximal effects is not always possible. These issues will be discussed qualitatively in section IV. The possibility that D_s, k_q, and Δ are controlled by proximal histidine–heme steric interactions is discussed in Appendix A, in the context of hemoglobin cooperativity.

To complete this section we must evaluate the static distribution function, $P(a)$, induced by the quenched protein fluctuations ($T < T_f$). We also show how averaging over the fluctuations at high temperature ($T > T_f$) leads directly to an intuitive single exponential (Arrhenius) limit.

We utilize eq 19 and assume, as implied by eq 18a and 18b, that the protein fluctuations can be described by a quasiharmonic approximation.[20] The probability distribution of x can be written as

$$P_q(x) = \left[\frac{f}{2\pi k_B T}\right]^{1/2} \exp[-fx^2/2k_BT] \text{ (quintet)} \quad (29a)$$

$$P_s(x) = \left[\frac{f}{2\pi k_B T}\right]^{1/2} \exp[-f(x - x_0)^2/2k_BT] \text{ (singlet)} \quad (29b)$$

for temperatures above the freezing point where entropic factors have overcome the local energy minima associated with the protein solvent potential.[17] The force constant f is related to the protein–solvent, protein–protein potential which is taken as harmonic in the simplest approximation. A detailed description of the phase transition region is complicated by the fact that the system is usually frozen while in the bound state (singlet) configuration. Thus $P_s(x)|_{T=T_f}$ describes the low-temperature distribution of x. As the system begins to melt and diffusion in the x coordinate is allowed, the probability density will migrate to $P_q(x)$ (see ref 7 for a discussion of this issue). We will not present the detailed diffusion analysis here, but rather consider that the diffusion coefficient of the coordinate x is either zero (below T_f) or very large (above T_f). The effects of intermediate values of diffusion will be qualitatively discussed in the last section. Using eq 19 and 29b we find that the distribution of a is Gaussian at the freezing point and below

$$P(a) = P_s(a) = \left[\frac{1}{2\pi\sigma_a^2}\right]^{1/2} \exp[-(a - a_0^*)^2/2\sigma_a^2] \quad (30)$$

with

$$\sigma_a^2 = \frac{\alpha^2 k_B T_f}{f} \quad (31)$$

For temperatures above T_f, where fluctuations are rapid in comparison to the rebinding, we must average the rates over x

$$\langle k \rangle = \int P(x)k(x)\,dx \quad (32)$$

After integration of eq 32 and some algebra, it can be seen that $\langle k \rangle$ depends explicitly on the quantity α^2/f. This unknown ratio can be conveniently eliminated by use of eq 31, leading to

$$\langle k \rangle = k_0' e^{-E_A/k_BT} \quad (33a)$$

with

$$E_A = H_D + \tfrac{1}{2}Ka_0^2(1 + K\sigma_a^2/k_BT_f)^{-1} \quad (33b)$$

and

$$k_0' = k_0(1 + K\sigma_a^2/k_BT_f)^{-1/2} \quad (33c)$$

Here we have used eq 31 to replace α^2/f with σ_a^2/k_BT_f. Equations 32 and 33 have not explicitly addressed the issue of bounded diffusion by the protein.[7] If $P(x)$ is taken to be $P_s(x)$, this implies no protein diffusion and a_0 is given by the low-temperature value, a_0^*. If, on the other hand, we allow for rapid protein diffusion at high temperature, $P(x)$ should be replaced by $P_q(x)$ in eq 32. This leads directly to a new value for a_0 at high temperature

$$a_0^\dagger = a_0^* - \alpha x_0 \quad (34)$$

Such an analysis seems justified (even at the expense of the extra parameter), since it is unlikely that the iron relaxes to the full out-of-plane position in the low-temperature photoproduct. For Mb·CO we estimate that $\alpha x_0 \cong -0.1$ Å so that $a_0^* \cong 0.35$ Å and $a_0^\dagger \cong 0.45$ Å.

Thus, we can use the parameters from the low-temperature kinetics experiments to predict, with some certainty, the value of E_A obtained at high temperature

$$H_D + \tfrac{1}{2}Ka_0^{*2}(1 + K\sigma_a^2/k_BT_f)^{-1} < E_A < H_D + \tfrac{1}{2}Ka_0^{\dagger 2}(1 + K\sigma_a^2/k_BT_f)^{-1} \quad (35)$$

where we estimate T_f to be in the vicinity of 200 K. It turns out (vide infra) that eq 33–35 are in excellent agreement with the observed high-temperature rates. Finally, we can use eq 31 and 34 to find a relation for global conformational energy

$$\tfrac{1}{2}fx_0^2 = \tfrac{1}{2}k_BT_f(a_0^\dagger - a_0^*)^2/\sigma_a^2 \quad (36)$$

This energy can be compared directly to a localized iron–porphyrin binding energy, $^1/_2k_qa_0^{*2}$, in order to assess the relative importance of these terms. Using the parameters discussed above with $\sigma_a = 0.11$ Å (Table I) and $k_q = 17$ N/m (Table III), we find $^1/_2fx_0^2 \sim 0.68$ kJ/mol and $^1/_2k_qa_0^{*2} \sim 6.3$ kJ/mol, which justifies dropping the x-dependent terms in eq 16 and 17 as discussed prior to eq 20.

III. Data Analysis

We utilize both eq 11 and 15 in the analysis of the rebinding data.[22a] A formal interpretation of the fitting parameters (K, H_D, and σ_a^2) is derived in eq 26–31. The parameters a_0^* and $a_0^\dagger$ are directly obtained either from X-ray, which yields $a_0^\dagger = 0.45$

(22) (a) The data used in section III are supplied by the group of H. Frauenfelder and prepared for our use by P. Steinbach. (b) The data for β-hemoglobin (βHb·CO) rebinding have also been provided and fit using the present model. It appears that the noise in the βHb·CO data is significantly larger than that in the case of Mb·CO or Lb·CO. The fact that the $g(H)$ distribution for βHb·CO is found at relatively small values of H indicates that much of the experimental information is carried by the short time ($<10^{-6}$ s) kinetics. We find that the existing data set does noes uniquely specify the $g(H)$ distribution. One parameter set, consistent with the data, is given as follows ($\chi^2 = 5.78 \times 10^{-2}$): $H_D = 1.63 \times 10^{-2}$ kJ/mol, $K = 10.3$ N/m, $a_0^* = 0.35$ Å, $\sigma_a = 0.13$ Å, $k_0 = 8.5 \times 10^8$ s^{-1}. Other more radical parameters sets can be generated, giving equivalent χ^2 values. The fits are visually similar to those displayed in ref 8. It is worth noting that, when H_D is small, eq 33b can predict a significant *decrease* in the high-temperature Arrhenius barrier height, E_A, relative to the energy barrier at the maximum of $g(H)$. This arises when $K\sigma_a^2/k_BT_f$ is of order unity or larger. In such a case, the peak of the distribution is found at $H_{max} \sim {}^1/_2Ka_0^2$, while the high-temperature limit is given by $E_A \sim {}^1/_4Ka_0^2$. This situation is consistent with the parameter set given above for βHb·CO. The reported values[5] for βHb·CO are $H_{max} \sim 3.6$ kJ/mol and $E_A \sim 1.8$ kJ/mol. The magnitude of the reported change[5] (ca. a factor of 5) in k_0 for βHb·CO between low and high temperature is more difficult to interpret within the present model. (However, the values of k_0 may not be unambiguously specified by the data.) We can only suggest that the dynamic and static limits may offer some difference in the frictional effects at work in this system.[18] Alternatively, one must always remain cautious when the uniqueness of the fits is suspect. The high-temperature extrapolations[5] in βHb·CO may also suffer from this problem, since it is not clear how uniquely the amplitudes for the various processes (e.g., matrix diffusion) are specified by the data. Subtle variations in these amplitudes could affect the values of $\langle k \rangle$ extracted from the data.

Table I. Parameters for Mb·CO Rebinding[a]

parameter	rebinding fit	independent values	independent technique
a_0*	0.35 Å	0.45 Å	X-ray diffraction[23,24]
		0.35 Å	EXAFS[26]
σ_a	0.11 Å	0.3 Å[b]	X-ray, T = 200 K[16,17]
		0.24 Å	Mössbauer, T = 200 K[17]
		0.25 Å	Soret absorption[12]
		0.07 Å	dynamics calculation[29]
K	13.8 N/m	5.1 N/m	Soret absorption[12]
		≥2.1 N/m[c]	Mössbauer[17]
		88 N/m	Raman $\tilde{\nu}_{Fe-N_{His}}$ = 220 cm^{-1}
k_0	2.8 × 10^9 s^{-1}		
H_D	7.0 kJ/mol	6.9 kJ/mol	high-temperature rebinding limit (via eq 33), $\langle H \rangle$ = 12.2 kJ/mol[8,36]

[a] Useful conversions: N/m = 10^{-2} mdyn/Å = 1.44 kcal/(mol Å^2), kcal/mol = 4.18 kJ/mol = 350 cm^{-1}. [b] The values of σ_{Fe} obtained from X-ray and Mössbauer spectroscopy are expected to be somewhat larger than σ_a. This is primarily because they are absolute rather than relative measures of iron disorder. [c] One cannot simply use the slope of σ_{Fe}^2 vs T in the linear region ($\sigma_{Fe}^2 \cong k_B T/K_{Fe}$) to extract the low-frequency force constant, since the coupling constants that relate the Cartesian and normal coordinates are also needed (see ref 41 for details). When the zero-point contributions to σ_{Fe}^2 are analyzed, the coupling constant for the low-frequency mode(s) can be determined to be on the order of 0.1 (P. Debrunner, private communication). This sets a lower limit of $K \geq 2$ N/m from Mössbauer spectroscopy.

Table II. Fitting Parameters and Their Uncertainties[a] for Mb·CO Rebinding

a_0* (Å)	σ_a (Å)	k_0 (GHz)	K (N/m)	H_D (kJ/mol)	χ^2[b]
0.45	$0.15^{+0.06}_{-0.05}$	$2.9^{+3.0}_{-1.5}$	$8.3^{+6.5}_{-2.8}$	7^{+2}_{-4}	3.94 × 10^{-3}
0.35	$0.11^{+0.05}_{-0.04}$	$2.8^{+3.0}_{-1.5}$	$13.8^{+10.2}_{-4.8}$	7^{+2}_{-4}	3.93 × 10^{-3}
0.25	$0.08^{+0.04}_{-0.03}$	$2.9^{+3.0}_{-1.5}$	$26.9^{+19.1}_{-10.0}$	7^{+2}_{-4}	3.94 × 10^{-3}

[a] Uncertainty Δp in a fitting parameter p is defined in the following way: if one of the parameters, p, is changed by an amount Δp and all other parameters optimized for minimum χ^2, then the new value of χ^2 is 1.5 times greater than the value listed above. [b] χ^2 is defined as

$$\chi^2 = \sum_{i=1}^{n_{pt}} \left[\frac{N(t_i) - N_{calc}(t_i)}{\sigma(t_i)} \right]^2 / (n_{pt} - n_{par})$$

where $N(t_i)$ and N_{calc} (t_i) are the values of $N(t)$ measured and calculated at time t_i, respectively, $\sigma(t_i)$ are weighting factors for $N(t_i)$ ($\sigma(t_i) = N(t_i)$ in the fitting procedure), n_{pt} is the number of points and n_{par} the number of fitting parameters (n_{par} = 4). If a percentage estimate for the error $\sigma(t_i)$ in $N(t_i)$ is utilized, a "normalized" χ^2 is easily obtained. For example, 1% error in $N(t_i)$ leads to reduction in σ by 10^2 and an increase in χ^2 by 10^4.

Å for deoxy Mb,[23,24] or from EXAFS, which suggests a_0* = 0.35 Å for the low-temperature Mb photoproduct.[26]

Figure 4 shows the rebinding data for Mb·CO (pH 7.0) over many orders of magnitude in time and at a number of different temperatures. The dashed curves represent the error function approximation of eq 15 and the solid curves are the result of integration of eq 11. We find that eq 15 is particularly useful in the early stages of the fitting procedure and allows the parameters to be determined quite accurately before the integral (eq 11) is used in the final calculations. In Table I we list the parameters used to fit the rebinding data of Mb·CO. Three sets of parameters are listed in Table II in order to demonstrate the

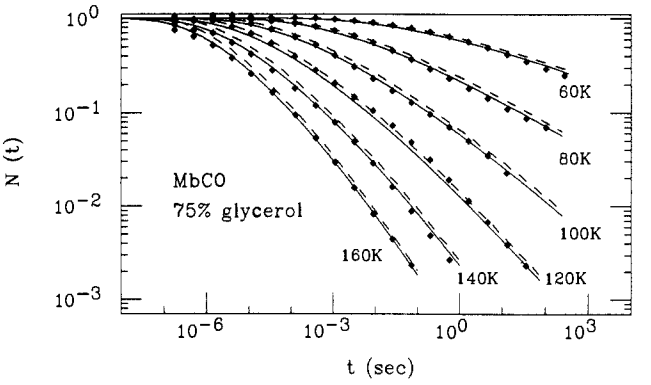

Figure 4. A fit, using the model presented here, of the rebinding kinetics of CO to sperm whale myoglobin (Mb·CO) at low temperature.[22] The dashed curves are the fit with the closed form approximation (eq 15) and the solid curves are the fit with the exact integral (eq 11). For this fit a_0* = 0.35 Å and all other parameters are listed in Table I.

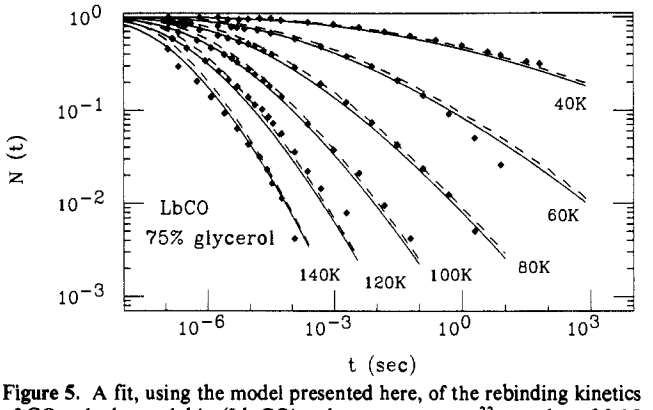

Figure 5. A fit, using the model presented here, of the rebinding kinetics of CO to leghemoglobin (Lb·CO) at low temperature.[22] A value of 0.35 Å is used for a_0* and other parameters are the following: k_0 = 3.12 × 10^9 s^{-1}, σ_a = 0.073 Å, K = 16.25 N m^{-1}, H_D = 1.15 kJ mol^{-1}. Solid and dashed lines are the same as in Figure 4.

systematic effect of varying a_0*. The most appropriate value, given the experimental conditions,[22a] is probably a_0* = 0.35 Å for the photoproduct Mb*. Alternative experimental arrangements[7] involving a true deoxy initial state (freezing under illumination) would more properly employ a_0* = $a_0^{\dagger}$ = 0.45 Å. Data from other independent measurements are also displayed in Table I and the comparisons will be discussed in the next section. Generally, we find that the parameters are well determined by the low-temperature rebinding data, once a_0* is fixed.

In Table II we list the χ^2 between theory and experiment and show how the fits deteriorate when the parameters are individually perturbed from their preferred values. The results indicate that, in order to stay within ~50% of the χ_{min}^2, the parameters must be specified to within a factor of 2.

In Figure 5 we display the fits to another set of data involving leghemoglobin (Lb). We choose Lb·CO recombination because the observed kinetics are distinct from Mb·CO. The parameters are listed in the figure caption and again the fits are quite satisfactory. Additional fitting of other existing data sets should be straightforward within this model.[22b] Since we do not wish to pursue the detailed fitting of numerous data sets, we display in Figures 6 and 7 a variety of the distributions $g(H)$ that have been found[25] using the technique of numerical inverse Laplace transformation of $N(t)$.

In Figure 6 we compare the $g(H)$'s from eq 10 with the numerical inverse Laplace determined counterparts. The agreement indicates, in some sense, the "uniqueness" of a given $g(H)$. A divergence at $H = H_D$ is an artifact that arises when we plot $g(H)$ rather than the true probability, $g(H)\,dH$, which is finite at $H = H_D$. The divergence is eliminated in the figure in favor of the "average" $g(H)$ between H_D and H_{min} (see caption of Figure 6). Figure 7 shows a variety of $g(H)$ functions as determined by the

(23) Takano, T. J. Mol. Biol. 1977, 110, 569–584.
(24) Phillips, S. J. Mol. Biol. 1980, 142, 531–554.
(25) Reinisch, L. Ph.D. Thesis, University of Illinois, 1982.
(26) Powers, L.; Chance, B.; Chance, M.; Campbell, B.; Friedman, J.; Khalid, S.; Kumar, C.; Naqui, A.; Reddy, K. S.; Zhou, Y. Biochemistry 1987, 26, 4785–4796.
(27) Bangcharoenpaurpong, O.; Schomacker, K. T.; Champion, P. M. J. Am. Chem. Soc. 1984, 106, 5688–5698.

Table III. Binding Potential Parameters and Experimental Constraints[a]

parameter	key relationship	experiment	best estimate
k_s, k_q	$\sigma_{s,q}^2 = k_B T/k_{s,q}$	EXAFS vs T[b] optical vs T[c]	62 N/m (k_s)[30] 17 N/m (k_q)
R_D	$K = [(2R_DR_k + 2R_D + 1)/((2R_D + 1)(2R_DR_k + 1))]k_q$	low-temp kinetics ($R_k = k_q/k_s$ from above)	0.82
Δ_v	$H_D = \Delta_v/(2R_D + 1)$	low-temp kinetics ($R_D = D_s/D_q$ from above)	18 kJ/mol
D_s	$D_s = \Delta H + \Delta_v + {}^1/_2 k_q a_0^2$	high-temperature kinetics[2] $\Delta H \equiv V_q(a_0,\infty) - V_s(0,0) \cong$ (90 ± 2) kJ/mol	115 kJ/mol
β	$2\beta^2 D_s = k_{Fe\text{-}CO}$	Raman: $\bar{\nu}_{Fe\text{-}CO}$ = 510 cm^{-1} $k_{Fe\text{-}CO}$ = 288 N/m	2.8 Å^{-1}

[a] The six free parameters of the rebinding potential are constrained by various independent relationships that involve experimentally determined quantities. Four of the six needed relationships have reasonable experimental constraints. Only the quantities k_s and k_q are needed to uniquely specify the potential surface. The quantity a_0 is extracted from X-ray analysis. [b] May be difficult to extract if doming and/or orientational effects are involved in the coordinate Q. Vibrational spectroscopy is also a possibility, but the effective mass is difficult to determine. [c] Broadening of the optical spectra[12] may also show a temperature dependence due to this effect.

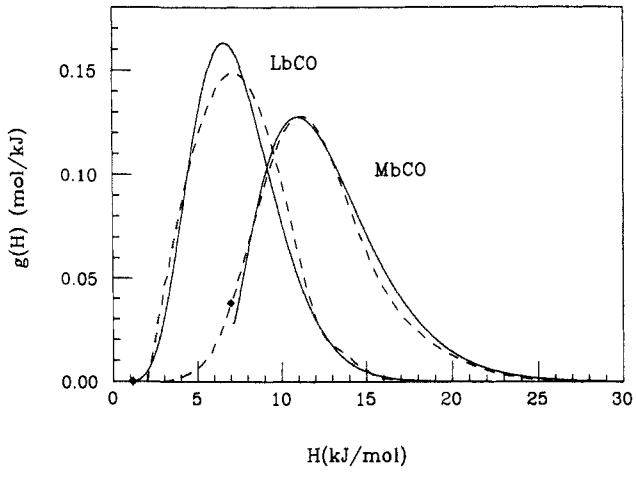

Figure 6. The activation enthalpy probability distributions, $g(H)$, for the CO recombination to leghemoglobin (Lb·CO) and sperm whale myoglobin (Mb·CO) (both at pH 7). The solid lines are from the model presented here (eq 10) applied to recombination data of Frauenfelder's group.[22] Parameters used to determine these distributions are the same ones used in the fits of Figures 4 and 5. The divergence in $g(H)$ at $H = H_D$ is not shown. Instead, diamonds at the beginning of the $g(H)$ curves represent $\int_{H_D}^{H_{min}} g(H)\, dH/(H_{min} - H_D)$, where H_{min} is the minimum in the G(H) curve in the vicinity of H_D. (For Mb·CO: H_D = 7 kJ/mol and H_{min} = 7.1 kJ/mol; for Lb·CO: H_D = 1.15 kJ/mol and H_{min} = 1.17 kJ/mol). The diamond therefore represents the average of $g(H)$ between H_D and H_{min}. We can average over this narrow range of enthalpy since it corresponds to a resolution that is finer than that of the experiment. The dashed lines are from a smoothed (cubic spline) 32-point numerical inverse Laplace transform (see ref 25 for details). The pre-exponentials for the numerically determined distributions are $k_0 = 2.2 \times 10^9$ s^{-1} for Mb·CO and $k_0 = 4.4 \times 10^9$ s^{-1} for Lb·CO. The solid and dashed line distributions provide equally good fits to the measured data.

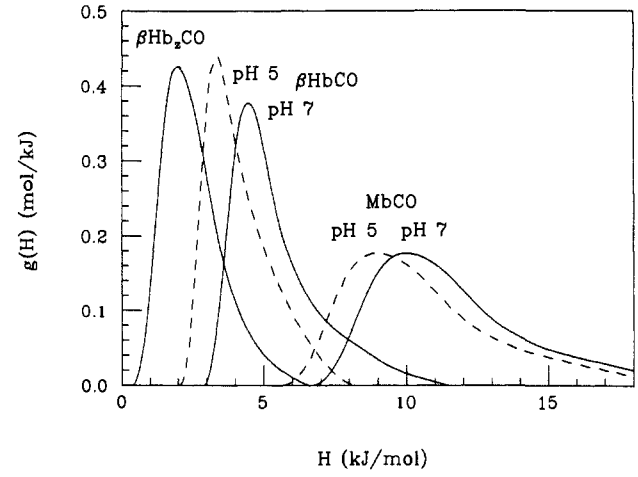

Figure 7. The activation enthalpy probability distributions, $g(H)$, for heme protein CO recombination. The distributions were generated from a smoothed 32-point numerical inverse Laplace transform, applied to the measured $N(t)$ recombination. The distributions for the recombination of CO to the sperm whale myoglobin (Mb·CO) and separated β chains of the normal adult (βHb·CO) and mutant Zürich (βHb$_z$·CO) human hemoglobin are taken from ref 25 and shown for two values of pH. (For βHb$_z$·CO, the distribution is pH independent.) All distributions have been normalized such that $\int_0^\infty g(H)\, dH = 1$. The distributions in Figure 6 differ slightly from the Mb·CO distributions presented in Figure 7 because in Figure 6 we used recombination data for times 10^{-7} s $\leq t \leq$ 10 s, whereas the distributions of Figure 7 use data only in the range 2 × 10^{-6} s $\leq t \leq$ 10 s. The extended time domain of the data set used to generate the previous figure allows a better value for the pre-exponential to be determined. Unfortunately, only the limited time range data are available as a function of pH.

inverse Laplace transform technique. The main point to stress here is that the shift along the H-axis, observed for the various compounds in Figure 7, is controlled by H_D in the current model. The additional energy needed to bring the iron atom to the in-plane transition state gives breadth to the curves and leads to the distributed kinetics. Thus, we postulate that variations in H_D along with the proximal work, H_P, control the mean barrier height and regulate the binding kinetics. Possible sources of systematic variation of H_D will be discussed in the next section.

IV. Discussion

A. Parameter Space. 1. a_0*. When the fitting parameters listed in Table I are compared with other independent measurements, the results seem quite reasonable. The value of a_0* is most straightforward, since this parameter can be directly measured with X-ray[23,24] or EXAFS[26] techniques. We let a_0* = 0.35 Å as suggested by EXAFS studies[26] of Mb*, the low-temperature photoproduct. In anticipation of the possibility that better refinement of the EXAFS data may lead to smaller values for a_0*, we have also listed in Table II the parameter set that is associated with a_0* = 0.25 Å. Alternative experimental arrangements,[7] involving cooling of the irradiated (deoxy) sample, would more properly employ the a_0 as found from X-ray studies of deoxy crystals (a_0 = 0.45 Å). As can be seen from the values of χ^2 in Table II, the overall fits to the data are of comparable quality. Generally, the decreased values of a_0*, associated with Mb*, result in a reduced value for σ_a and a larger K. In a more elaborate model, that explicitly includes protein diffusion, one could incorporate the possibility that the iron atom relaxes to different positions, $a_0(T)$, as a function of temperature. Diffusion effects are considered here only in the high-temperature limit so that $a_0(T < T_f) = a_0$* and $a_0(T > T_f) = a_0^\dagger$.

2. σ_a. The parameter σ_a may also, in principle, be determined through independent sets of experiments. Unfortunately, experiments involving the combination of Mössbauer and X-ray

studies[16,17] do not lead directly to a determination of σ_a. The ambiguity arises from several sources: (1) correlated motion of the iron and porphyrin, (2) averaging effects due to random orientations, and (3) differences in the fluctuation spectrum between solution Mb and crystalline Mb.

Point 1 involves the possibility that the iron and porphyrin can move together without affecting their relative positions. Point 2 involves the anisotropic nature of the system and the fact that the kinetics (within this model) probes only the coordinate of motion perpendicular to the porphyrin plane. Point 3 arises from suggestions[28] that the dynamic behavior of the protein may be hindered in the crystal by packing forces. Thus, estimates of σ_a based on X-ray analysis may not be appropriate for the solution kinetic studies.

It appears that an alternative experimental determination of σ_a might involve careful EXAFS studies. Concerns 1 and 3 are directly eliminated but an analogue of point 2 remains, i.e., the extraction of a small z component of disorder from a much larger radial distance. Even more serious problems arise when the insensitivity of EXAFS to doming of the porphyrin is considered (i.e., when the iron moves out of plane, the nitrogen coordination shell moves with it). Further theoretical and experimental work along these lines may be justified, but for now we must be content that the values for $\sigma_a \sim 0.1$ Å seem "reasonable" in view of the measured X-ray and Mössbauer values for σ_{Fe}. Recent protein dynamics studies[29] have, in fact, predicted that $\sigma_a \sim 0.07$ Å in reasonable agreement with the results of Table I. Insofar as a_0^* is reduced to ~0.25 Å the kinetic analysis is consistent with even smaller values of $\sigma_a \sim 0.08$ Å (see Table II).

3. K. The parameter K presents an important challenge with respect to independent determination. This parameter is tied, through eq 26, to the details of the potential energy surface. It may be possible to improve our understanding of such details by employing additional experiments and/or calculations. Warshel, for example, has calculated energy surfaces[30] that allow estimates of the force constants $k_q \cong 17$ N/m and $k_s \cong 62$ N/m (from Figure 3, ref 30). These parameters lead directly to $R_k = 0.27$ and allow the unique determination of all other parameters of the potential energy surface. In Table III, we delineate some key equations and possible experiments that can be used to constrain the final shape of the potential surface. Our best estimate for the potential surface is also given.

This should give impetus to experiments that can monitor σ_Q^2 versus temperature (Q = q or s). The dynamic quantity σ_Q^2 must be distinguished from σ_a^2, which is the static distribution of "equilibrium" positions. Since the contributions of correlated low-frequency motion such as bulk heme displacements parallel to the plane (points 1 and 2 discussed above) will also be observed when only the iron atom motion is monitored, it seems that Mössbauer experiments will have difficulty in directly extracting the important parameters k_q and k_s. Mössbauer measurements could be used to set an upper limit on σ_Q^2, assuming that the coupling coefficients between the Cartesian and normal modes can be found (see footnote c, Table I). Once again we might turn to careful EXAFS measurements as a function of temperature and hope to extract the dynamic Debye–Waller terms $\sigma_Q^2 \cong k_B T/k_{s,q}$ directly from the analysis. However, the inability of EXAFS to detect a dynamic "doming" motion of the heme may also prove to be a limiting factor in this type of analysis. Studies of spectral line broadening as a function of temperature[12] could provide further insight, insofar as the relative iron–porphyrin coordinate can also affect the energy of certain optical transitions.

4. k_0. We now briefly turn to the "prefactor", k_0, which is not so intimately tied to the detailed potential energy surface. Frictional effects, as well as the entropy changes upon binding, are usually included in this term. When friction is important and the binding is considered to be adiabatic,[18] it may be useful to calculate the slopes (forces) of the q and s state potential surfaces in the direction of reaction. In this respect, the parameters used to model the potential can be used to estimate characteristic length-scales[18] which help to determine self-consistent limits on the parameter space.

The probability for making the electronic change of state on a single crossing can also be included in the prefactor. For the spin alterations involved in heme–ligand binding, this will involve spin–orbit coupling to first ($\Delta S = 1$) or second ($\Delta S = 2$) order. The first-order coupling is expected to be much larger and may help to explain ligand binding studies that involve triplet-state intersections. For example, the binding of molecular oxygen can be considered within the present two-surface model by simply replacing V_s with an analogous surface for the triplet state (V_t) as suggested by valence bond theory.[19] So long as friction is neglected, the major effect will be carried in larger values of k_0, reflecting the first-order spin–orbit matrix elements. However, the near equivalence of k_0 for the CO and O_2 binding reactions at low temperature suggests the importance of friction and/or undetected intermediate states.[18] An alternative possibility is that oxygen binding, which ultimately results in a system singlet state, actually involves second-order spin–orbit coupling terms. A more subtle interaction may be indicated by recent studies involving isocyanides.[31] We suggest that a genuine triplet intersection (q → t → s) may occur when a strong σ-donating ligand perturbs the d_{z^2} orbital of iron. Thus, the observed[31] rapid geminate rebinding may be due to the large first-order matrix elements in the intersection region, even though the final singlet state of Mb·CNR is analogous to Mb·CO.

5. H_D. The final unknown parameter in the analysis, H_D, is quite important in the overall control of the rebinding kinetics. Equation 28 is a general statement of some of the potential sources of variation in H_D. The factor $R_D = D_s/D_q$ is especially important in this regard, since it is sensitive to the strength of the Fe–CO bond (through D_s) as well as the CO–quintet state repulsion energy (through D_q). The parameter Δ_v is correlated with the crystal field environment of the iron and can be affected via significant protein conformational changes (e.g., T → R transition in Hb). In this respect, the classification of the first term in eq 28 as a purely "distal pocket" effect is somewhat ambiguous, since both the distal and proximal structure can affect this term.

We note that recent spectroscopic studies have found a linear correlation between the Fe–CO and C–O stretching frequencies.[32a] This is almost certainly due to a variation in the amount of Fe → CO π-back-donation into the π^* orbitals of CO. The correlation is also shown to extend to the dissociation rate constants and this implies that D_s increases with increasing k_{Fe-CO} as expected. The source of these effects has been attributed to a variation in the off-axis Fe–C–O bond angle (θ). When $\theta = 0$, and the system is in a linear geometry, it is suggested[32a] that less d_π(Fe) → π^*(CO) donation takes place. When the bond is tilted ($\theta \neq 0$) more d_π–π^* overlap is postulated and a stronger Fe–C and weaker C–O bond results. An alternative suggestion[32b] is that distal pocket polarization effects may systematically vary the amount of electron density in the π^* orbitals of CO. The bond angle analysis has been qualitatively applied to the rebinding data[33] in order to account for some of the systematic variation in the values of H_D obtained for different heme proteins such as found in Figure 7.

One of the key experimental observations is that systems having higher Fe–CO frequencies also have *larger* H_D's. For example, we have found[33,34] that the Fe–CO stretching frequency of Mb

(28) Krupyanskii, Y. F.; Parak, F.; Goldanskii, V. I.; Mössbauer, R. L.; Gaubman, E. E.; Engelmann, H.; Suzdalev, I. P. *Z. Naturforsch.* **1982**, *37c*, 57–62.
(29) Nadler, W.; Brünger, A. T.; Schulten, K.; Karplus, M. *Proc. Natl. Acad. Sci. U.S.A.* **1987**, *84*, 7933–7937.
(30) Warshel, A. *Proc. Natl. Acad. Sci. U.S.A.* **1977**, *74*, 1789–1793.
(31) Jongeward, K. A.; Magde, D.; Taube, D. J.; Marsters, J. C.; Traylor, T. G.; Sharma, V. S. *J. Am. Chem. Soc.* **1988**, *110*, 380–387.
(32) (a) Uno, T.; Nishimura, Y.; Tsuboi, M.; Makino, R.; Iizuka, T.; Ishimura, Y. *J. Biol. Chem.* **1987**, *262*, 4549–4556. (b) Li, X.; Spiro, T. *J. Am. Chem. Soc.*, submitted.
(33) Champion, P. M. *International Symposium on Frontiers in Science*; Chan, S., Ed., in press.
(34) Reinisch, L.; Šrajer, V.; Champion, P. M. *Bull. Am. Phys. Soc.* **1987**, *32*, 1412.

shifts from 490 to 510 cm^{-1} as the pH is raised from 5 to 7. The corresponding upward shift in the $g(H)$ curves can be seen in Figure 7. The observation of a simultaneous increase in bond strength along with an *increased* barrier height is difficult to explain by using only a simple variation in the Morse binding potential. Since D_s must increase to simulate a stronger bond, eq 28 would predict a *decrease* in H_D so long as D_q is held constant ($R_D = D_s/D_q$). However, if we assume that D_s and D_q are *both* functions of geometry (θ) and/or polarization (χ), the observations can be simply explained. If the effect of nonlinear orientation and pocket polarization is to increase $D_s(\theta,\chi)$ through π-back-donation, an even larger increase in $D_q(\theta,\chi)$ is dictated by the rebinding data (i.e., R_D must decrease so that H_D increases along with D_s).

Distal pocket "sticking" forces or other energy associated with displacement of distal residues[35] are a third source of possible variation in H_D. Such effects can be included in the quantity H_S in eq 28. It is worth noting that analogous arguments also support the observation of slightly smaller values of H_D in the O_2 complexes. This is due to the lack of geometric or steric strain in the naturally bent oxy complexes.

B. Comparisons to Previous Theory. A number of previous investigations[7-11] have focussed on the theoretical analysis of the Mb·CO rebinding data. We do not give a complete review here, but simply comment on some of the relevant similarities and differences between the previous work and the present model.

The works of Agmon and Hopfield[7] (AH) and Young and Bowne[8] (YB) follow a similar logic that can be directly compared with the present model. Both previous approaches[7,8] describe the entire protein with a probability density that involves a single generalized coordinate, X, which is "frozen out" below T_f. The crucial iron–porphyrin coordinate (Q) considered here is not separated from X and this results in a fundamental difference in the predicted dynamics below T_f. In contrast to the previous models, the heme is free to relax through Q in the present model, and *energetically significant* local heme motion is accounted for even at low temperature. For example, in the AH model it seems that the iron atom must remain fixed during the low-temperature binding process. Even when the AH model is considered within the "sudden" approximation, where the iron atom is allowed to move instantly to its new equilibrium position, there can be no energetic consequences within the confines of the AH potentials. A typical approach to the transition state in the AH model is shown as a dashed line in Figure 2, where the coordinate Q is absorbed by X and held fixed throughout the binding process at low temperature.

At higher temperatures in the AH theory, bounded diffusion in the X coordinate sets in. The probability density then begins to migrate (diffuse) toward the equilibrium position of the deoxy protein with increasing speed (i.e., it is no longer fixed throughout the course of the rebinding trajectory). This leads to an initial slowing down of the reaction at intermediate values of the diffusion constant before a simple exponential process takes over at the highest temperature.[7] The Arrhenius (high-temperature limit) energy barrier, E_A, is then found to be considerably larger than the energies associated with the distributions $g(H)$. This is due to the extra energy associated with the conformational rearrangements in going from the "reactant" protein configuration, with $X = 0$, to the "product" protein configuration ($X = X_0$). In contrast, the present model associates the main effect of protein diffusion with a temperature-dependent a_0. We have considered explicitly only two limiting cases, $a_0^*(T < T_f) \cong 0.35$ Å and $a_0^\dagger(T > T_f) \cong 0.45$ Å; however, a complete solution to the diffusion equation could be used to predict $a_0(T)$ and study its correlations with temperature-dependent optical spectra.

The overall difference in a_0 between low and high temperature is quite important in determining the value of E_A calculated from the low-temperature distribution. For example, eq 35 sets stringent limits on the Arrhenius energy barrier. After evaluating the terms in eq 35, using the low-temperature kinetic parameters ($a_0^* = 0.35$ Å, $a_0^\dagger = 0.45$ Å), we find

$$10.2 \text{ kJ/mol} < E_A < 12.3 \text{ kJ/mol} \quad (37)$$

which is quite close to the experimentally measured[8,36] high-temperature value of the total binding enthalpy (12.2 ± 1.0 kJ/mol). Small differences, <2 kJ/mol, may be due to "H_B", the enthalpy between CO in solution and in the protein pocket. The close agreement with the upper limit, $E_A = 12.3$ kJ/mol, indicates the validity of the approximation involving rapid diffusion from $a_0^* = 0.35$ Å to $a_0^\dagger = 0.45$ Å when $T > T_f$. On the other hand, if we choose an alternative set of parameters with $a_0^* = 0.25$ Å (see Table II), more iron diffusion is necessary when $a_0^\dagger = 0.45$ Å. This leads to an upper limit value of E_A (17 kJ/mol) which is not so compatible with the experimental high-temperature rate. The parameter set with no protein diffusion ($a_0^* = a_0^\dagger = 0.45$ Å) leads to $E_A = 10$ kJ/mol. These results indicate that the kinetic measurements at low[2] and high[36] temperature are quite consistent with the EXAFS determined[26] value, $a_0^* = 0.35$ Å for photolyzed Mb. In contrast to the AH model, which suggests $E_A = 32.6$ kJ/mol for Mb·CO,[7,8] it appears that the predicted value of E_A, measured at high temperature, does not increase significantly beyond the energy where $g(H)$ reaches a maximum value; in fact, there may even be a *decrease* of E_A in the case of βHb·CO.[5,22b] The successful high-temperature extrapolation speaks strongly for the present model.

In the intermediate regime diffusion is slow, but non-zero. In this case, each molecule will begin to experience a number of (fluctuation driven) Fe–porphyrin equilibrium positions during the rebinding reaction. On the average they should remain centered around $a_0(T)$, however, and we do not foresee a "slowing down" of the reaction at intermediate values of the diffusion constant. In this respect, we believe that the experimentally observed slowing down of the reaction at intermediate temperature[1-6] may, in fact, correspond to the motion of CO away from the pocket and into the protein matrix.

The issue of the apparent decrease in normalization $N(t)$ (i.e., recombination on time scales less than 10^{-9} s) for certain systems (e.g., protoheme) is also stressed in the AH development. This arises from the fact that no relaxation in X is possible within their model and, for certain values of X, the system can never cross into the quintet potential surface. This occurs when there are large displacements between initial and final equilibrium positions (large X_0). Once again we note that the fixed X condition, in the absence of an explicit coordinate Q, suggests that the iron–porphyrin geometry remains fixed during the photolysis and subsequent rebinding step. The present model allows for the relaxation of the system to $Q = a$ and the unhindered variation of Q will always give the system access to the quintet surface. This will subsequently lead to unit normalization. However, if severe steric hindrance of the relaxation in Q is involved, and a_0^* is small, similar arguments can be made to reduce the normalization at $t \sim 10^{-6}$ s due to ultra-fast recombination events. It is conceivable that the absence of the globular protein material in the "bare" protoheme does lead to more constraint of the iron–prophyrin coordinate (i.e., the frozen solvent maintains the iron atom in the "in-plane" configuration so that very rapid geminate recombination ensues). Another possible source of "normalization" effects might involve intersections of the triplet-state surface. Such added complications will not be discussed here.

The work of Buhks and Jortner[9] treats the very low temperature kinetics[3] in a one-dimensional non-adiabatic model that can account for tunneling and quantum effects. However, no attempt is made to include the effects of distributions. It is actually this work that first stimulated our interest in the relevance of the iron–porphyrin coordinate. Our original goal was to include the

(35) Moffat, K.; Detherage, J. F.; Seybert, D. *Science* **1979**, *206*, 1035–1042.

(36) Doster, W.; Beece, D.; Bowne, S. F.; DiIorio, E. E.; Eisenstein, L.; Frauenfelder, H.; Reinisch, L.; Shyamsunder, E.; Winterhalter, K. H.; Yue, K. T. *Biochemstry* **1982**, *21*, 4831–4839.

(37) Alberding, N.; Austin, R. H.; Chan, S. S.; Eisenstein, L.; Frauenfelder, H.; Gunsalus, I. C.; Nordlund, T. M. *J. Chem. Phys.* **1976**, *65*, 4701–4711.

distributions in coupling strength and calculate the rebinding as a function of time for all temperatures, including the quantum effects. This basically amounts to the calculation of a Franck–Condon broadened absorption band as a function of temperature. The zero frequency ($\tilde{\nu} = 0$) absorption intensity then gives the relevant Franck–Condon matrix element as a function of temperature. While such techniques are standard for harmonic surfaces and optical frequencies (ref 12 and references therein), they are difficult to apply in practice (when $\tilde{\nu}$ is far from the absorption maximum) and are not well suited for the dissociative and anharmonic surfaces of the r coordinate. The differing masses associated with motion in the r and Q directions also complicate the full quantum mechanical calculation. (However, certain WKBJ methods may be applicable.[38])

Work along similar lines by Bialek and Goldstein[11] holds to linear coupling of a one-dimensional surface and introduces distributions via anharmonic perturbations of the quadratic terms (i.e., the force constants are distributed throughout the ensemble). The single mode calculations lead to sharp structure in the Franck–Condon spectrum (transmission function), so that small shifts in mode frequency "detune" the zero-frequency component and lead to large changes in the rebinding rate. In addition to the nonadiabatic premise,[18] there appear to be two main problems with this model: (1) The damping is kept extremely small ($\gamma = 0.01$ cm^{-1}) in order to obtain the needed sharp structure in the spectrum. This seems inconsistent with observed vibrational line widths (10 cm^{-1}) and decay times. (2) The sharp structure is also the result of recurrences in the correlator that will be (self) damped once the presence of more than a single mode frequency is acknowledged. When points 1 and 2 are considered, and the Franck–Condon spectrum is broadened out, it seems unlikely that a distribution of force constants will be such an effective means for distributing the rates. The lack of observable "hole-burning" in the Fe–N_{His} Raman mode[39] also suggests that distributions in the quadratic coupling are quite small.

C. Summary and Future Outlook. In summary, it appears that a simple intuitive picture of proximal and distal pocket work can go a long way toward explaining the observed rebinding data of CO to myoglobin. The more formal generalization of this approach allows the kinetically determined parameters to be combined with the results of other experiments in order to map out the detailed structure of the relevant potential energy surface. Table III indicates how the various experimental measurements can lead to a unique determination of the surface. As it stands, we are remarkably close to a unique determination. The key variables that need to be restricted by further experiments are k_q and k_s. If these quantities were known, the potential surface would be uniquely specified. Definition of a distal boundary potential would then justify complete phase space or even tunneling calculations. Use of calculated[30] values for k_q and k_s leads directly to the "best estimate" parameter values listed in Table III.

The effect of the protein fluctuations has been restricted to distributions of the linear coupling which are *localized* at the heme. Such effects are not unexpected and recent calculations by Elber and Karplus[40] have shown that a large number of thermally accessible minima are in the neighborhood of the "native" structure. It is important to recognize that the protein fluctuations are *globally* isoenergetic ($< k_B T$). Yet, the various local regions within the protein structure can increase and/or decrease energetically so long as the *sum* of all contributions remains within $\sim k_B T$ of the global minimum. We suggest that the distribution in the iron–porphyrin equilibrium position is driven by such fluctuations of the protein conformation between global minima near the "native" structure. The energy changes at the heme are thus balanced by changes in energy of other regions in the protein. This basic idea, that the *local* energetics of the heme can be modulated by protein conformational changes that are thermodynamically favorable (or accessible) in the *global* sense, has been previously discussed in the context of hemoglobin cooperativity.[27] This idea is further developed in Appendix A with use of explicit potential energy surfaces. In the case of Mb, where isoenergetic fluctuations rather than cooperative structural rearrangements govern the changes, we suggest that a fluctuation driven distribution of iron–porphyrin "equilibrium" positions leads directly to the nonexponential rebinding kinetics observed at low temperature.

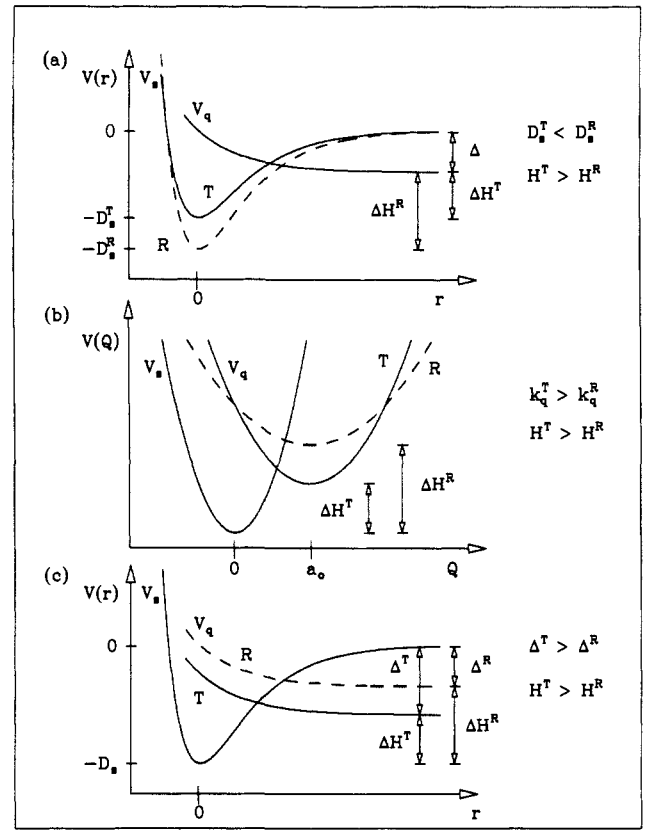

Figure 8. The effects of changing parameters D_s, k_q, and Δ on the potential surface. Changes in these parameters can be associated with the T → R transition in hemoglobin. In all cases the T → R transition leads to a lower barrier height ($H^T > H^R$) and, therefore, to a higher rate for ligand binding to the R-state. Part a shows the effect of a change in the depth of the Morse bound-state potential, D_s, part b the effect of a change in the force constant of the deoxy, quintet surface, k_q, and part c the effect of a change in Δ, the stabilization energy of quintet state for large r. In all cases the heme localized binding enthalpy ΔH, which governs the affinity for ligand binding, is altered by a change in the corresponding parameter. These cases represent different ways of changing the local heme affinity in the T → R transition: stabilizing the ligand bound R-state surface (a) or destabilizing the deoxy R-state surface (b, c).

In the model of Agmon and Hopfield, the global protein energy of the q and s states plays a much more dominant role than in the present theory. This is because the internal iron–porphyrin coordinates are not explicitly considered during the binding process. The present model allows for internal relaxation (through the coordinate Q) and assigns the major differences between the q and s states to the change in equilibrium position of Q. If additional differences in the q and s state conformational energy (at fixed x) are included in the model (through the x-dependent terms of eq 16 and 17), they can be incorporated by a more general interpretation[21] of the fitting parameters a_0 and H_D (the very general eq 7–11 still hold, however). It seems that the x-dependent conformational energies are more relevant in the analysis of cooperative proteins such as Hb (see Appendix A).

Finally we suggest that more work needs to be done concerning the effects of the triplet state. The present experimental data do

(38) Widom, A.; Clark, T. D. *Phys. Lett.* **1983**, *93A*, 217–218.
(39) Campbell, B. F.; Chance, M. R.; Friedman, J. M. *Science* **1987**, *238*, 373–376.
(40) Elber, R.; Karplus, M. *Science* **1987**, *235*, 318–321.
(41) Housley, R. M.; Hess, F. *Phys. Rev.* **1966**, *146*, 517–526.

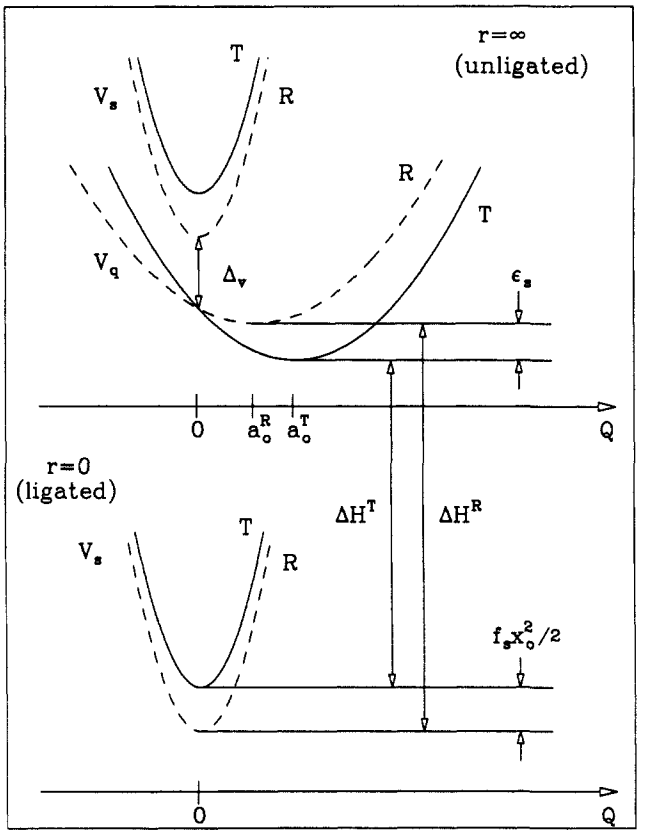

Figure 9. The Q-dependence of the potential energy surfaces of the iron atom in the R (dashed) and T (solid) states. The delocalized steric and electrostatic energy, due to binding when the protein is held in the unligated (T) conformation, is also shown ($^1/_2 f_s x_0^2$). Small changes in a_0 and K_q lead to a significant difference ($\epsilon_s \sim 1.5$ kcal/mol) between the Stokes shifts of the two quintet ground states at $r \rightarrow \infty$ (upper panel). As $r \rightarrow 0$ the singlet state follows a Morse potential and becomes the ground state (lower panel). The enthalpies of binding (ΔH^T, ΔH^R) are affected by both ϵ_s and the delocalized heme–protein interactions involving electrostatic and steric effects ($^1/_2 f_s x_0^2$). The vertical electronic gap (Δ_v) between the q and s states of the iron atom is held constant at $Q = 0, r \rightarrow \infty$ (i.e., $\Delta_v^T = \Delta_v^R$ in order to demonstrate the importance of the Stokes shift alone. Note that the apparent difference in the vertical energies at $Q = 0$ in the upper panel is not due to a change in Δ_v but rather due to the protein specific terms, $^1/_2 f_s x_0^2$, that have been added to the diagram. In this sense, the vertical axis of the figure represents a *total* system energy, not just the energy of the iron electronic states and their nuclear distortions. The magnetic susceptibility experiments discussed in the text probe only iron electronic states and are generally insensitive to the $^1/_2 f x_0^2$ terms. Thus, the stabilization energy of the high-spin T electronic state versus the R-state (i.e., $\Delta^T > \Delta^R$) leads to the larger high-spin fraction observed in the bound T-state materials. Conformationally induced electronic perturbations of the singlet state are possible, but much less likely. This is due to the correlated motion of the iron and porphyrin in the hexacoordinate complex, which isolates the crystal field of the bound iron atom from protein conformational change.

not yet warrant these more general considerations. However, it is conceivable that the triplet state may play an important role in the rebinding process. In the case of oxygen binding it is still possible to utilize eq 16 and 17, if the singlet state is simply replaced by a triplet state. In the event that all three states are involved, a more complicated intersecting potential surface must be considered. Further study of the general effects of spin-dependent terms in the Hamiltonian is also needed.

We hope that the picture presented here can serve as a starting point for more elaborate calculations as well as a reference point for further experiment. For example, the present model should be able to quantitatively account for recent "hole burning" observations involving the 760-nm band of deoxy Mb.[39] It seems evident that direct correlations must exist between σ_a, $a_0(T)$, and certain structurally sensitive optical transitions.[12,39] Moreover, as the potential energy surface becomes better defined through

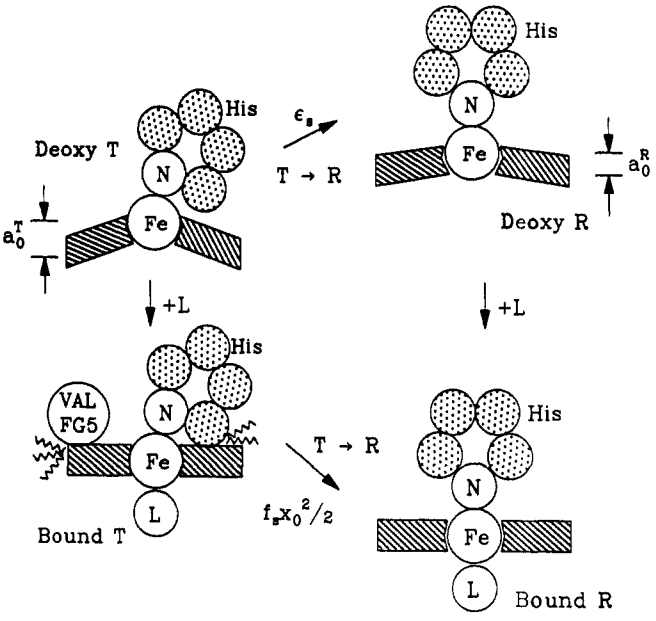

Figure 10. A schematic picture of the four key states involved in the phenomenon of Hb cooperativity. Some of the increased energy of the unligated R-state is localized at the heme iron and involves the electron–nuclear coupling (Stokes shift, ϵ_s) and pure electronic crystal field alterations. Such changes will be reflected in iron localized experiments such as magnetic susceptibility where the high-spin T-state is found to be stabilized with respect to high-spin R-state. The strain and electrostatic energies ($^1/_2 f_s x_0^2$) are global and found primarily in the ligated T-state structure. Both effects can work together to increase the R-state ligand affinity. Continuous protein control of the Stokes shift, through the iron–porphyrin equilibrium position, can lead directly to a more sophisticated model of cooperativity where the binding enthalpy is not strictly quantized.

experiment, we should also be able to extrapolate into the tunneling regime and predict the very low temperature kinetics.[3,4] The effects of different heme ligands can also be expressed through a ligand specific variation of the potential surface parameters (e.g., D_s, k_s, D_q, H_D). This might help to form a consistent framework for the quantitative discussion of the wide variety of kinetic and thermodynamic experiments that have been performed on heme proteins. Such an approach should be useful in quantifying the effects of protein-induced perturbations of the heme structure (and local energetics) and should clarify their functional role in certain catalytic and electron-transfer events as well as in the simple ligand binding reactions.

Acknowledgment. This work was supported by NIH DK 35090 and NSF DMB 84-17712. One of us (P.M.C.) is the recipient of a NIH Research Career Development Award (AM 01405). We are grateful for several illuminating discussions with Peter Debrunner concerning the interpretation of Debye-Waller factors obtained from Mössbauer spectroscopy. Peter Steinbach, Hans Frauenfelder, and Noam Agmon are especially thanked for supplying us with the rebinding data and for critical readings of the manuscript.

Appendix A: The Cooperativity of Hemoglobin

Potential surfaces of the type shown in Figures 2 and 3 are also useful in the description of heme localized changes associated with the T → R transition of hemoglobin. Figure 8 delineates the specific effects of certain key parameters used to describe the potential surfaces. The sections through the surface depict either the Fe–ligand coordinate (r) or the Fe–porphyrin coordinate (Q). Typical T-state potentials are shown as solid lines and changes in the surfaces, associated with the T → R transition, are shown as the dashed lines for the R-state surface.

Changing the individual parameters can be seen to alter the barrier height (i.e., $H^T > H^R$) and the heme localized binding enthalpy ($\Delta H^T < \Delta H^R$) in all cases. This affects the kinetics of reaction and the equilibrium constant or "affinity". The binding

enthalpy is altered by stabilizing the ligand bound R-state singlet surface ($D_s^R > D_s^T$) or by destabilizing the deoxy R-state quintet surface ($\Delta^R < \Delta^T$ or $k_q^R < k_q^T$).

For example, the effect of the parameter D_s is shown in part a of the figure. This situation associates differences in the T and R heme binding enthalpies with stabilization of the ligand bound R-state heme via the local iron-ligand bond energies. Certain proximal histidine–heme interactions could conceivably account for this effect. However, we suggest that "trans" interactions of this type may not play such a major role in the determination of the Fe–CO Morse potential and its depth. Ligand-dependent electronic factors and distal pocket constraints[35] are a much more likely source of such effects. In the case of Hb·CO it seems that the stability of the Fe–CO covalent bond is unaffected by the T → R transition. This view is supported by the fact that $\tilde{\nu}_{Fe\text{-}CO} \sim \beta\sqrt{D_s}$ is independent of quaternary structure.[42]

A more likely role of the proximal histidine–heme interaction would be to increase the *forces* associated with moving the iron atom into the heme plane.[43] Such an effect can be modelled by increasing k_q so that $k_q^T > k_q^R$. It can be seen from part b of the figure that this will affect the binding kinetics by changing the barrier height and, for a constant amount of linear coupling ($a_0^T = a_0^R$), it will affect the affinity (or equilibrium constant) due to the force constant dependence of the Stokes shift ($^1/_2 k_q a_0^2$). Another likely effect of the histidine–heme, protein–heme interaction would be to alter the equilibrium displacements of the two quaternary structures so that $a_0^T > a_0^R$.

Part c of Figure 8 demonstrates the overall effect of differences in Δ as viewed along the r coordinate. It must be remembered that $\Delta = \Delta_v + {}^1/_2 k_q a_0^2$ and the vertical transition energy (Δ_v) is held constant in the absence of pure electronic effects. The nuclear relaxation energy (Stokes shift) is quite strongly affected by linear coupling of the type discussed in the text. Namely, a_0 is significant ($\sim$0.35–0.45 Å) and should be dependent upon gross conformational rearrangements, just as $a(x)$ depends upon protein fluctuations about the mean (see Figure 9). We note that an earier treatment[27] has discussed cases where Δ_v may also have conformational dependence, insofar as the crystal field of the pentacoordinate iron atom is affected by different relative orientations of the histidine–heme system.

In addition to affecting the Stokes shift of the deoxy state, another important role of the proximal histidine–heme, protein–heme interaction has been discussed by Gelin and Karplus.[44] This involves the delocalized protein forces that are set up in the T-state structure when ligands bind. Such forces involve not only the proximal histidine but also the key pyrole III vinyl group interaction with Val FG5. These forces lead to strain energy which is present in the *ligated* T-state structure but absent in the unligated complex. This strain energy, along with the (linear and quadratic) interactions discussed above for the *unligated* state, ultimately leads to the stabilization of the R-state quaternary structure and the breaking of the intersubunit salt bridges as more ligands bind.

Warshel and Weiss[45] have calculated upper limits to the strain energy term and find $\Delta G_s < 2$ kcal/mol, assuming no protein relaxation upon ligand binding. In addition, these authors have estimated the effects of electrostatic stabilization of the more positively charged ligated heme and find that the R-state structure can accommodate such charge more effectively than the T-state. It is suggested that the T-state structure may be destabilized by as much as $\Delta G_e \sim 1$ kcal/mol due to the electrostatic effects. Taken together, the electrostatic and strain forces can be approximated to yield a relative R-state stabilization energy of $\sim$2 kcal/mol. (Here we have assumed that $\Delta G_s \sim 1$ kcal/mol by allowing for some protein relaxation upon binding.[45]) These terms alone do not appear to be sufficient to account for the observed difference in binding energies $\Delta G_R - \Delta G_T \sim 3.6$ kcal/mol, the so-called "energy of cooperativity".

In the order to clarify the remaining description, we first consider the simplt two-state model of cooperativity which involves the following: (1) local T-state ligand binding, (2) global quaternary structural change T → R, and (3) local R-state ligand binding. More general considerations, involving the progressive weakening of salt bridges and continuous variations in free energy of binding, will be considered qualitatively below. The thermodynamics of the individual ligand binding steps 1 and 3 will be considered in the context of the potential surfaces described by eq 16 and 17 of the text. Typical surfaces are shown in Figures 2 and 3. A schematic of the overall situation is shown in Figure 10. The Q-dependence of the unligated and bound states, along with the x-dependent steric and electrostatic term, is displayed in Figure 9.

In the case of myoglobin rebinding *kinetics* we have shown that the x-dependent terms in eq 16 and 17 can be dropped under the condition $^1/_2 f x_0^2 \ll {}^1/_2 k_q a_0^2$. On the other hand, in order to understand the energetics of cooperativity we must consider these terms more carefully. The T → R structure change in Hb clearly involves much more dramatic alterations in x than the small, fluctuation-driven, conformational perturbations of Mb. In this respect, we acknowledge that ligation to the T-state subunit involves additional strain energy since the surrounding protein does not completely relax until the T → R switch takes place. Thus, we associate the protein state $\langle x \rangle = x_0$ with the R structure (average protein coordinate of bound state, eq 29b). In similar fashion, we let $\langle x \rangle = 0$ stand for the T-state structure (unligated protein conformation, eq 29a). The brackets around $\langle x \rangle$ remind us that we are concerned here with a room temperature "average" structure and not the fluctuations that affect the kinetics below T_f.

The calculations of Gelin and Karplus as well as Warshel and Weiss support the view that the heme–protein interaction forces are felt primarily in the *bound* T-state and not in the unligated state. Thus, we let $f_s \gg f_q$ in eq 16 and 17 so that the bound T-state structure is destabilized by $^1/_2 f_s x_0^2$ with respect to the R-state (eq 18b with $x = 0$ for T and $x = x_0$ for R). The x-dependent terms in eq 17 and 18a are seen to have negligible effect on the energetics (and the rebinding kinetics) since f_q is small, as assumed previously for myoglobin. Using the calculations of ref 45, we estimate $^1/_2 f_s x_0^2 \sim 2$ kcal/mol of destabilization energy for each heme bound in the T-state structure.

The additional interaction that arises naturally from the potential surfaces of eq 16 and 17 involves the Stokes shift of the (unligated) quintet surface. This energy shift occurs due to changes in the iron–porphyrin force constant or equilibrium position. The linear part of this energy shift is *spectroscopically silent* with respect to Raman frequency, which probes only the *relative* spacing of vibrational energy levels. The general insensitivity of the porphyrin ring Raman modes to small second-order structural effects (such as alterations in the iron–porphyrin equilibrium) has been discussed previously.[46] Small motions of the pyrrole nitrogens along with the iron atom, associated with a $\sim$0.1 Å change in the iron–porphyrin equilibrium, are observed[47] to alter the heme ring modes by only 2–3 cm^{-1}. Such changes are compatible with the Raman spectra of the R and T forms of carp Hb.[46] Moreover, recent detailed Raman studies of quaternary structure induced changes in a variety of deoxy[48] and ligated[49] hemoglobins have associated much larger spectral shifts with the deoxy species. This is in complete accord with the hypothesis that the unligated heme is more flexible in its response to the changing tertiary environment induced by either the fluctuations or the quaternary structural change. In ligated hemoglobins the bonds and interactions associated with the heme are "tighter" and thus

(42) Tsubaki, M.; Srivastava, R. R.; Yu, N. T. *Biochemistry* **1982**, *21*, 1132–1140.
(43) Perutz, M. F. *Proc. R. Soc. London, Ser. B.* **1980**, *208*, 135–162.
(44) Gelin, B. R.; Karplus, M. *Proc. Natl. Acad. Sci. U.S.A.* **1977**, *74*, 801–805.
(45) Warshel, A.; Weiss, R. M. *J. Am. Chem. Soc.* **1981**, *103*, 446–451.
(46) Scholler, D.; Hoffman, B. *J. Am. Chem. Soc.* **1979**, *101*, 1655–1662.
(47) Dasgupta, S.; Spiro, T. *Biochemistry*, **1986**, *25*, 5941–5948.
(48) Ondrias, M.; Rousseau, D.; Shelnutt, J.; Simon, S. *Biochemistry* **1982**, *21*, 3428–3437.
(49) Rousseau, D. L.; Tan, S. L.; Ondrias, M. R.; Ogawa, S.; Noble, R. W. *Biochemistry* **1984**, *23*, 2857–2865.

do not respond as much to the changing quaternary structure.[49]

On the other hand, quadratic coupling effects can be observed more easily by studying Raman frequency shifts. Small increases in the Fe–N_{His} mode frequency have been observed upon T → R conformational changes.[50,51] These shifts translate to a ca. 5–10% increase in the Fe–N_{His} force constant and presumably reflect the absence of histidine–porphyrin steric repulsion in the R state that strains the Fe–His bond in the T state. Since the iron–prophyrin mode is at much lower frequency and involves motion of the histidine, iron, and pyrrole nitrogens, along with part of the F helix, it must have less covalent character. Thus, we expect that the histidine–porphyrin steric repulsion can easily lead to a ca. 10–20% increase of k_q^T over k_q^R.

We now proceed within the following simple hypothesis. We suppose that the mean equilibrium position of the iron–porphyrin coordinate is smaller in the unligated R-state than in the *T*-state. Thus, we let $a_0^R \simeq 0.35$ Å and $a_0^T \simeq 0.45$ Å which is consistent with Raman observations and is supported by EXAFS studies[52] and by the optical analysis of the Soret band red shift observed in the T → R transition.[12] Recent X-ray diffraction studies of model compounds[53a] and R-state deoxy hemoglobin[53b] confirm this hypothesis. Differences in coupling in the R and T states may well be controlled by protein conformation through interactions such as the proximal histidine tilt and orientation. The expressions for Δ, which carry the Stokes shift, are given by

$$\Delta^T = \Delta_v^T + \tfrac{1}{2}k_q^T(a_0^T)^2 \qquad \text{(A1a)}$$

$$\Delta^R = \Delta_v^R + \tfrac{1}{2}k_q^R(a_0^R)^2 \qquad \text{(A1b)}$$

where the case $k_q^T = 1.2\ k_q^R$ is depicted in Figure 9. Here we take $\Delta_v^T = \Delta_v^R = \Delta_v$ and assume that the crystal field of the unligated iron atom at $Q = 0$ is independent of quaternary state. The upper part of Figure 9 shows the ground-state deoxy surfaces, V_q, for the unligated R and T states at $r \to \infty$ along with the excited singlet state surface. The lower panel shows only the bound singlet surface, V_s, at $r = 0$ after binding takes place. (One can imagine the singlet surface following the Morse potential into the page and down to the lower panel while the quintet surface at $r = 0$ is repelled out of the figure.) The delocalized effects involving the steric and electrostatic terms are carried by the extra factor, $^1/_2 f_s x_0^2$, associated with the ligated T-state tertiary structure. The relative Stokes shift between the R and T state deoxy surfaces is given by

$$\epsilon_s = \tfrac{1}{2}k_q^T(a_0^T)^2 - \tfrac{1}{2}k_q^R(a_0^R)^2 \qquad \text{(A2)}$$

If we now use reasonable estimates[30] for $k_q^R \simeq 17$ N/m and $k_q^T \simeq 20$ N/m and let $a_0^R = 0.35$ Å and $a_0^T = 0.45$ Å we find

$$\epsilon_s \simeq 1.5 \text{ kcal/mol} \qquad \text{(A3)}$$

where ca. 1 kcal/mol comes from linear coupling and 0.5 kcal/mol from the quadratic effects. It should be noted that the energetic contribution from the unligated T and R states can be even larger when pure electronic effects are considered and $\Delta_v^T > \Delta_v^R$ as discussed previously.[27]

It appears that such effects may have already been observed experimentally.[43,46] In cases where the bound ligand allows for thermal accessibility to the high-spin surface, magnetic susceptibility measurements of spin equilibria probe differences between Δ^T and Δ^R (see Figure 8c at $r = 0$). As mentioned above, differences in D_s^T and D_s^R (Figure 8a) appear unlikely for Hb·CO. In fact, magnetic studies of the R and T forms of various types of ferric Hb indicate that the T-state high-spin surface is stabilized by about 1 kcal/mol with respect to the R-state high-spin surface.[43] More detailed analysis of available susceptibility and Raman data is needed in the context of the present potential surfaces, but the general experimental results strongly support the present hypothesis. The basic point is that heme localized control by the protein is much more likely to be manifested in the *unligated* T and R subunits where fluctuations and conformational change can alter the *ground* state energy via Δ. Differences between Δ^T and Δ^R are then reflected directly in the enthalpy of binding.

As an illustration of the two-state model, we calculate total free energy change at an arbitrary state of ligation ($i = 0, 1, 2, 3, 4$). We first note the approximately $\Delta G° = RT \ln L = 8.8$ kcal/mol is needed to switch T → R with no ligands present[54] ($L = [Hb]_T/[Hb]_R$). Of this, $4\epsilon_s$ must be used to overcome the local differential in energy of the four unligated hemes. The rest of this energy must be due to independent global terms, ΔG_{globin}, involving hydrogen bonds, salt bridges, entropy, etc. Thus, we write:

$$\Delta G^i_{T\to R} = \Delta G_{globin} + (4 - i)\epsilon_s - i(f_s x_0^2/2) \qquad \text{(A4)}$$

where we have assumed that $D_s^R = D_s^T$ as found from the Fe–CO Raman frequencies. The heme delocalized steric and electrostatic energy, associated with ligated T-state subunits, is carried by the term $f_s x_0^2/2 \sim 2$ kcal/mol.[44,45] The $i = 0$ limit sets $\Delta G_{globin} = 2.8$ kcal/mol when $\epsilon_s = 1.5$ kcal/mol as estimated above (eq A3). Solving for i when $\Delta G^i_{T\to R} = 0$ gives

$$i = 2.5 \qquad \text{(A5)}$$

which is close to the observed state of ligation at the switching point.[54] We stress that the above calculation is for illustrative purposes only and the values used for ϵ_s and $f_s x_0^2/2$ are only approximations based on calculations of k_q, ΔG_s, and ΔG_e that might have large uncertainties.

A more complex model of cooperativity involves a gradual weakening of the salt bridges and hydrogen bonds as successive ligands bind. Presumably, this leads to small, but measurable, changes in protein structure up to the point ($i \sim 2.5$) where major T → R alterations take place. Such effects are manifested in detailed studies of the free energy of ligation as a function of the number of ligands bound.[55] Since the binding free energies associated with successive ligation steps are not strictly quantized, we must consider how the protein might compensate its structure following the binding of each ligand. Within the present model, we could allow the value of a_0 to be a function of overall salt bridge composition and, thus, a function of the total number of bound ligands (i.e., $a_0 = a_0^i$). The two-state model is recovered by allowing $a_0^{0,1,2} = a_0^T$ and $a_0^{3,4} = a_0^R$. Thus, one can directly employ the present model to understand the more subtle control associated with the gradual weakening of the salt bridges. The associated change in the Stokes shift, $^1/_2 k_q(a_0^i)^2$, will then govern the small changes in the free energy of binding that are measured as a function of ligation state.

Next we consider how the experimental differences in the "on" and "off" rates for the R and T forms of Hb can be used to independently partition the 3.6-kcal/mol energy of cooperativity between the terms associated with the unligated and ligated states. Eaton and co-workers[56] have demonstrated that most of the relative difference in the "overall" binding rates, $k_{on}^R/k_{on}^T \sim 60$, arises at the heme–CO barrier and is not due to diffusion control or gating as the CO enters the protein. Similarly, the difference in overall off rates, $k_{off}^T/k_{off}^R \sim 10$, is also controlled at the heme.[56] Within the present model, the relative rates can be estimated by

$$k_{on}^R/k_{on}^T \sim \exp(\epsilon_s/k_B T) \qquad \text{(A6a)}$$

and

$$k_{off}^T/k_{off}^R \sim \exp(f_s x_0^2/2k_B T) \qquad \text{(A6b)}$$

where we let $k_q \ll k_s$ and assume that H_D, D_s, and Δ_v are independent of quarternary state. In a more general analysis, addi-

(50) Friedman, J. M. *Science* **1985**, *228*, 1273–1280.
(51) Nagai, K.; Kitagawa, T.; Morimoto, H. *J. Mol. Biol.* **1980**, *136*, 271–289.
(52) Chance, M.; Parkhurst, L.; Powers, L.; Chance, B. *J. Biol. Chem.* **1986**, *261*, 5689–5692.
(53) (a) Momenteau, M.; Scheidt, W.; Eigenbrot, C.; Reed, C. *J. Am. Chem. Soc.* **1988**, *110*, 1207–1215. (b) Perutz, M. F.; Fermi, G.; Luisi, B.; Shaanan, B.; Liddington, R. C. *Acc. Chem. Res.* **1987**, *20*, 309–321.
(54) Hopfield, J. J. *J. Mol. Biol.* **1973**, *77*, 207–222.
(55) (a) Gibson, Q.; Edelstein, S. *J. Biol. Chem.* **1987**, *262*, 516–519. (b) Ackers, G. *Biophys. J.* **1980**, *47*, 331–346.
(56) Murray, L. P.; Hofrichter, J.; Henry, E.; Eaton, W. A. *Biophys. Chem.* **1988**, *21*, 63–76.

tional effects involving ligand specificity and quaternary state electronic factors ($\Delta_v^T \neq \Delta_v^R$) can also be considered. Using the experimentally determined values for the ratios at 298 K, we solve eq A6 for ϵ_s and $f_s x_0^2/2$ to find

$$\epsilon_s \sim 2.4 \text{ kcal/mol} \quad \text{(A7a)}$$

$$f_s x_0^2/2 \sim 1.4 \text{ kcal/mol} \quad \text{(A7b)}$$

These values are in reasonable agreement with the theoretical estimates[30,45] used above. Additional refinement in the relative binding and dissociation rates can be accomplished by small variations in the other parameters (e.g., H_D, Δ_v, and D_s).

Further details involving diffusion control of the kinetics and ligand-dependent cooperative effects[35,57,58] will not be considered in quantitative detail at this time. However, the kinetic results involving carp Hb[58] are problematic, particularly since conclusions are based on a theoretical analysis[7] that has been shown[8] not to extrapolate to the high-temperature limit. An alternative[58] extrapolation of the low-temperature kinetics to the high-temperature regime may be flawed since it does not allow for protein diffusion when $T > T_f$. It seems that the low-temperature barrier height distributions for the R and T states may not be uniquely determined and, in any case, they have been incorrectly applied to calculate the high-temperature rates.[58] If we go beyond the simplified estimates of eq A6, we can derive the formal expressions for the barrier height, even for a more complicated molecule such as Hb. In this case we must acknowledge that $f_q \ll f_s$ (as discussed above) so that convenient substitution, $\alpha^2/f = \sigma_a^2/k_B T$, in eq 31-33 can no longer be made. Instead we calculate

$$E_A = H_D + \tfrac{1}{2} K a_0^2 (1 + K\alpha^2/f_q)^{-1} \quad \text{(A8a)}$$

$$k_0' = k_0(1 + K\alpha^2/f_q)^{-1/2} \quad \text{(A8b)}$$

If we now ask which of the deoxy structures is more flexible (the T or R state) we expect that $f_q^T > f_q^R$, reflecting the stabilization of the quaternary T-state structure due to the hydrogen bonds and salt bridges. From eq A8a we see that, when $f_q^T > f_q^R$, the extrapolation to high temperature will increase the barrier height more for the T state than for the R state. This is precisely the effect observed by Cobau et al.[58] Although a complete and careful reanalysis of the entire data set is probably called for, it is also noteworthy that these authors[58] find Δ^T to be significantly larger than Δ^R using the Agmon-Hopfield approach. This is further experimental evidence in support of the hypothesis that a significant amount of Stokes shift and/or crystal field electronic stabilization energy is present in the unligated T state of Hb.

(57) Szabo, A. *Proc. Natl. Acad. Sci. U.S.A.* **1978**, *75*, 2108-2111.
(58) Cobau, W. G.; LeGrange, J. D.; Austin, R. H. *Biophys. J.* **1985**, *47*, 781-786.

Determination of the Central Bond Length in Hexaarylethanes by Nutation NMR Spectroscopy

Nino Yannoni,*[1a] Bart Kahr,[1b] and Kurt Mislow*[1b]

Contribution from the IBM Almaden Research Center, San Jose, California 95120, and the Department of Chemistry, Princeton University, Princeton, New Jersey 08544.
Received January 15, 1988

Abstract: The lengths of the central bonds, r_c, in [α,α'-$^{13}C_2$]hexakis(2,6-di-*tert*-butyl-4-biphenylyl)ethane (**1**) and [α,α'-$^{13}C_2$]hexakis(3,5-di-*tert*-butylphenyl)ethane (**2**) have been determined by nutation NMR spectroscopy. The dipolar spectra obtained by this method were compared with computed spectra in which the central bond length was the only adjustable parameter. Best fits of the experimental and computed spectra were found to correspond to a r_c value between 1.64 and 1.65 Å for both compounds. These results are in excellent agreement with the X-ray value of r_c in **2** and provide the first direct experimental evidence that the reported[4] X-ray value of r_c in **1** is grossly in error.

Hexaphenylethane (HPE) has had an exceptionally colorful history for a molecule that has yet to be synthesized. For more than half a century following Gomberg's discovery of triphenylmethyl,[2] its dimer was believed to be HPE. It was not until 1968 that the correct structure of the dimer, first proposed by Jacobson in 1905, was elucidated by Lankamp, Nauta, and MacLean.[3] In 1978 Stein, Winter, and Rieker reported the first synthesis of an unbridged hexaarylethane, hexakis(2,6-di-*tert*-butyl-4-biphenylyl)ethane (**1**).[4] The X-ray structure of **1** featured the abnormally short central carbon-carbon bond length (r_c) of 1.47 (2) Å, a finding of no small import since just the year before we had reported our calculation, by the empirical force field method, of an abnormally long r_c (1.64 Å) for HPE.[5] A subsequent and more elaborate computational study[6] not only confirmed the original conclusions[5] in all essential details but predicted r_c = 1.64 Å (MM2) for **1** as well. Most recently we found[7] that r_c = 1.67 (3) Å in the X-ray structure of hexakis(3,5-di-*tert*-butylphenyl)ethane (**2**), a compound closely related to **1**. Moreover, the calculated (MM2) value of this parameter was 1.65 Å.[7]

In light of the computational studies[5-7] and the X-ray structure of **2**,[7] it would seem safe to dismiss the claim[4] for bond shortening in **1**. Nevertheless, with the single exception of the calculated

(1) (a) IBM Almaden Research Center. (b) Princeton University.
(2) Gomberg, M. *J. Am. Chem. Soc.* **1900**, *22*, 757; *Ber. Dtsch. Chem. Ges.* **1900**, *33*, 3150.
(3) Jacobson, P. *Ber. Dtsch. Chem. Ges.* **1905**, *38*, 196. Lankamp, H.; Nauta, W. Th.; MacLean, C. *Tetrahedron Lett.* **1968**, 249. See also: McBride, J. M. *Tetrahedron* **1974**, *30*, 2009.
(4) Stein, M.; Winter, W.; Rieker, A. *Angew. Chem.* **1978**, *90*, 737; *Angew. Chem., Int. Ed. Engl.* **1978**, *17*, 692. See also: Winter, W. *Fresenius' Z. Anal. Chem.* **1980**, *304*, 279. Winter, W.; Butters, T.; Rieker, A.; Butsugan, Y. Z. *Naturforsch.* **1982**, *37b*, 855. Winter, W.; Moosmayer, A.; Rieker, A. *Ibid.* **1982**, *37b*, 1623.
(5) Hounshell, W. D.; Dougherty, D. A.; Hummel, J. P.; Mislow, K. *J. Am. Chem. Soc.* **1977**, *99*, 1916. The AM force field was used: Andose, J. D.; Mislow, K. *J. Am. Chem. Soc.* **1974**, *96*, 2168.
(6) Ōsawa, E.; Onuki, Y.; Mislow, K. *J. Am. Chem. Soc.* **1981**, *103*, 7475.
(7) Kahr, B.; Van Engen, D.; Mislow, K. *J. Am. Chem. Soc.* **1986**, *108*, 8305. Correction: the included solvent molecules are located at Wyckoff *d*, a site of D_{2d} symmetry, rather than at Wyckoff *b*, a site of D_{2h} symmetry.

0002-7863/88/1510-6670$01.50/0